Spatial variability in salt marsh drainage controlled by small scale topography

Carmine Donatelli[1,2,*], Paola Passalacqua[1],

Daniel Jensen[3], Talib Oliver-Cabrera[3], Cathleen E. Jones[3], Sergio Fagherazzi[2]

Corresponding author: dcarmine@bu.edu

1. Department of Civil, Architectural and Environmental Engineering, University of Texas at Austin, Austin, TX, USA
2. Department of Earth and Environment, Boston University, Boston, MA, USA
3. Jet Propulsion Laboratory, California Institute of Technology, Pasadena, California, USA

Key points

1. We utilize a new generation of remote sensing data to study water movement beneath the vegetation canopy in salt marshes.
2. Small morphological features in marsh landscape affect the spatial variability in water drainage within vegetated areas.
3. Salt marshes located at the same elevation within the local tidal range drain water differently.

Abstract

Water movement in coastal wetlands is affected by spatial differences in topography and vegetation characteristics, as well as by complex hydrological processes operating at different time scales. Traditionally, numerical models have been used to explore the hydrodynamics in these valuable ecosystems. However, we still do not know how well such models simulate water-level fluctuations beneath the vegetation canopy, since we lack extensive field data to test the model results against observations. This study utilizes remotely sensed images of sub-canopy water-level change to understand how marshes drain water during falling tides. We employ rapid repeat interferometric observations from the NASA's Uninhabited Aerial Vehicle Synthetic Aperture Radar (UAVSAR) instrument to analyze the spatial variability in water-level change within a complex of marshes in Terrebonne Bay, Louisiana. We also use maps of herbaceous aboveground biomass derived from the Airborne Visible/Infrared Imaging Spectrometer-Next Generation (AVIRIS-NG) to evaluate vegetation's contribution to such variability. This study reveals that the distribution of water-level change under salt marsh canopies is strongly influenced by the presence of small geomorphic features (< 10 meters) in the marsh landscape (i.e., levees, tidal channels), whereas vegetation plays a minor role in retaining water on the platform. This new type of high-resolution remote sensing data offers the opportunity to study the feedbacks between hydrodynamics, topography and biology throughout wetlands at an unprecedented spatial resolution, and test the capability of numerical models to reproduce such patterns. Our results are essential to predicting the vulnerability of these delicate environments to climate change.

Keywords: salt marshes, water levels, vegetation, UAVSAR, AVIRIS-NG

Plain Language Summary

Salt marshes are vegetated coastal ecosystems particularly susceptible to lateral erosion and sea-level rise. Hydrodynamic models are crucial to forecasting the vulnerability of these delicate environments to climate change, but we lack extensive field data to assess the accuracy of such models in vegetated flooded areas. Here, we utilize measurements collected from a NASA radar instrument flown on an airplane to determine how water moves beneath the vegetation canopy within a group of salt marshes located in the Mississippi River delta plain, Louisiana. Plant structure in the selected marshes is estimated from an imaging spectrometer which flew near-simultaneously with the radar instrument. Our study shows the utility of remotely sensed data to comprehend wetland hydrodynamics at a very high spatiotemporal resolution, and improve the reliability of models that are needed to predict their fate.

1. Introduction

Salt marshes are vegetated landforms located at the boundary between land and sea. These valuable coastal ecosystems form in low-energy environments or near large rivers where fine sediments can accumulate [e.g., Fagherazzi et al., 2012]. Salt marshes provide crucial ecosystem services to coastal communities since they act as buffers against storms, serve as nurseries for commercial fisheries, and sequester carbon [e.g., Leonardi et al., 2018]. Their economic value has been estimated to be US$5 million per square kilometer in the United States [Costanza et al., 2014; 2017].

Despite their ability to adapt in response to external disturbances, many studies document that salt marshes are disappearing at an alarming rate around the world due to lateral erosion and drowning [e.g., Carniello et al., 2011; Marani et al., 2011; Schuerch et al., 2018; Xu et al., 2022]. Degradation of this precious habitat has a severe impact on coastal communities because it intensifies the risk of flooding and the impact of extreme events on cities and infrastructure [e.g., Temmerman et al., 2013; Orton et al., 2020].

Salt marshes expand or contract horizontally as a function of wind-waves and sediment availability, and they are potentially able to outpace sea-level rise through inorganic matter accumulation and organic mass production [Marani et al., 2007; 2010]. However, although organic matter allows vertical accumulation to offset sea-level rise [Mudd et al., 2010], salt marshes cannot rely on this contribution alone. In fact, if mineral fluxes are not the primary driver in marsh accretion (i.e. the organic part exceeds the inorganic one), marsh structural fragility and edge failure may occur [Peteet et al., 2018].

Mariotti & Fagherazzi [2010] argue that the rate at which salt marshes erode for a given wave climate and sea-level rise rate depends ultimately on sediment supply. If the sediment input from rivers and the coastal ocean is low, salt marsh collapse can occur even without sea-level rise. As such, the evaluation of sediment fluxes' direction and magnitude is fundamental to forecast the fate of salt marshes and determine their vulnerability to sea-level rise [e.g., Ganju et al., 2013; 2017]. To make reliable estimations, it is crucial to precisely quantify fluxes of water within these vegetated ecosystems and then focus on fluxes of sediments.

Until now, numerical modeling has been the primary tool to investigate water and sediment movements in coastal wetlands [e.g., Beudin et al., 2017; Xie et al., 2022]. However, numerical models of flooded vegetated areas may be unreliable, since we lack spatially distributed data to validate them. In fact, collecting field measurements beneath the vegetation canopy is challenging due to numerous practical limitations [e.g., Alsdorf et al., 2007].

Recently, remote sensing has been utilized to fill this data gap [e.g., Wiberg et al., 2020; Liao et al., 2020; Ayoub et al., 2016; Cathcart et al., 2020; Donatelli et al., 2023]. Airborne and spaceborne radars can perform multiple flights over the same region, allowing them to detect changes in sub-canopy water levels at a very high spatial resolution (5-10 meters) [e.g., Oliver-Cabrera and Wdowinski, 2016]. The Uninhabited Aerial Vehicle Synthetic Aperture Radar (UAVSAR) [Hensley et al., 2008; Fore et al., 2015] has the ability to perform rapid repeat interferometric surveys, offering a synoptic view of how water levels vary spatially with a revisit time of ~30 minutes [Oliver-Cabrera et al., 2021]. For instance, interferometric products measured by UAVSAR have been used to calibrate water levels over extensive wetland areas [Wright et al., 2022].

In this paper, we employ UAVSAR water-level change products derived from data collected during Delta-X campaigns [Jones et al., 2022]. So far, this dataset has been mainly used to correct bathymetric information derived from lidar [e.g., Wright et al., 2022; Zhang et al., 2022a; b]. Zhang et al. [2022a; b] proposed an iterative/empirical methodology which corrects bed elevation in wetlands by using the difference between observed and modelled water-level change. They assumed that lowering (increasing) bed elevation allows for more (less) tidal propagation and therefore larger (smaller) water-level change. However, as pointed out by the same authors, this approach, although it improves the accuracy of the model in reproducing changes in water level over time, can lead to unrealistic results for other hydrodynamic variables (e.g., flow velocities).

These UAVSAR observations open the possibility to study wetland hydrodynamics at a spatial and temporal resolution that has not been possible with other remote sensing platforms. Our goal is to utilize high-spatial resolution, remotely sensed maps of water-level change beneath the vegetation canopy to determine the factors influencing water movement in marshes during a falling tide. This analysis is particularly important for quantifying the resilience of marshes [e.g., French & Spencer, 1993; Sullivan et al., 2019; Pannozzo et al., 2021]. In fact, when water drains back to the ocean, nutrients and sediments are released within the surrounding environment with consequences for the long-term evolution of these vegetated ecosystems. Additionally, small creeks are typically ebb dominated because of the delay between water level and peak flow [Fagherazzi et al., 2008]. As such, water drainage in marshes is critical for the evolution of the tidal network.

We use a complex of salt marshes located in Terrebonne Bay, Louisiana, as a test case. Here, we address the following hydrodynamic questions: a) Do salt marshes characterized by the same elevation drain water differently? If so, what controls this difference? b) What is the role of vegetation in retaining water over marsh surfaces? c) Do small morphological features of the marsh landscape influence water-level change within the surrounding area? These questions are crucial to (i) understand water movement within these vegetated coastal habitats, and (ii) determine the level of detail required for topographic data to accurately simulate marsh hydrodynamics via numerical modeling.

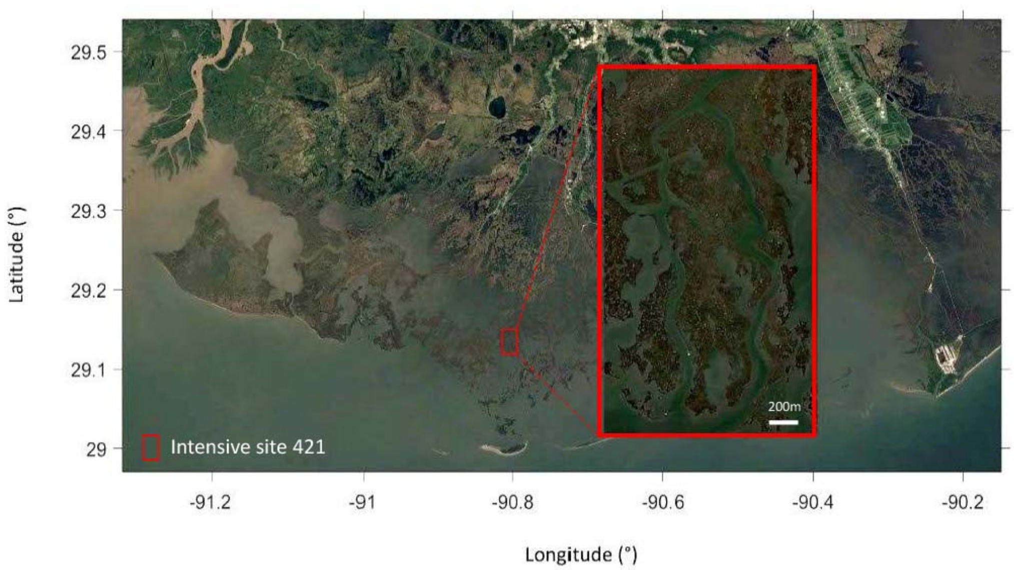

Figure 1. Satellite image of Terrebonne Bay, Louisiana, USA. The rectangle highlights the location of the three selected salt marshes (here, we call this location 'intensive site 0421').

2. Study site

Terrebonne Bay is a deltaic lagoon within the Mississippi Delta on the north coast of the Gulf of Mexico. Tides are diurnal with a mean astronomical tidal range of 0.32m. The system is strongly event-driven [Reed, 1989]. For instance, the effective tidal range reaches 0.7m by combining astronomical and meteorological components [Mariotti, 2016]. The bay presents a series of narrow and low-lying barrier islands (the Isles Dernieres and Timbalier chains) which separate the back-barrier basin from the Gulf of Mexico (Figure 1). The exchange of water between Terrebonne Bay and the coastal ocean occurs through tidal inlets, and it is affected mainly by tides and cold front passages [e.g., Reed et al., 1989]. Sediments needed for marsh accretion are derived from erosional processes occurring within the bay (e.g., bed erosion, marsh lateral erosion), and are delivered from offshore into the lagoon by storms [Cortese & Fagherazzi, 2022]. The lagoon is located between the Mississippi River Delta and the Atchafalaya Delta (Figure 1). The presence of these two systems creates differences in vertical stratification of the water column between the eastern and western parts of the bay. Such differences influence biological processes within Terrebonne Bay and are highly variable due to seasonal changes in wind conditions [Hetland & Di Marco, 2007].

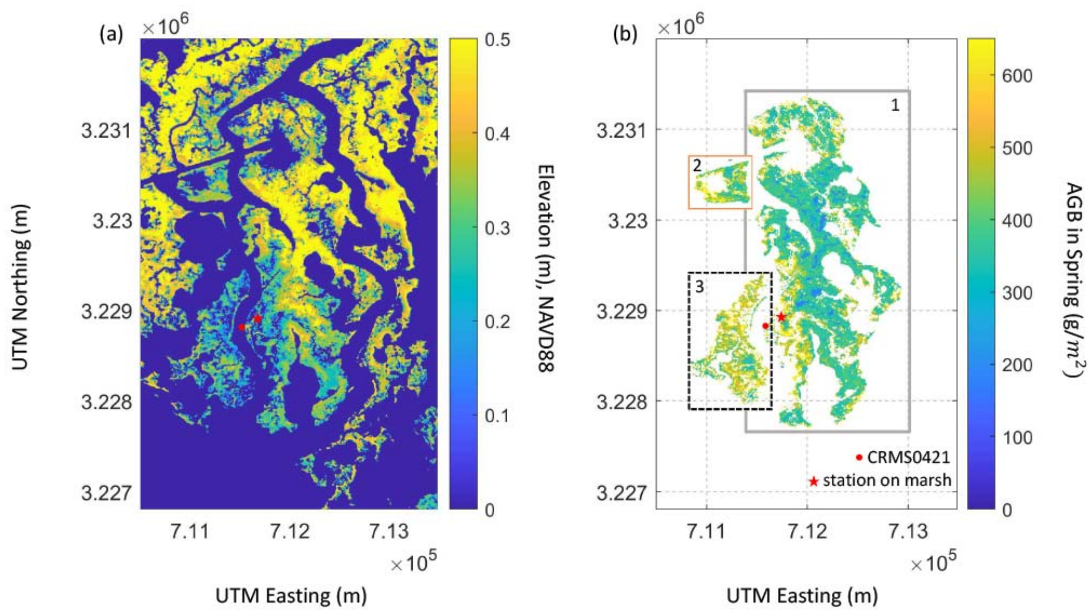

Figure 2. (a) Topography of the study site. Topographic data are reported with respect to NAVD88. (b) Above ground biomass (AGB) in spring. The (orange) thin lines and the (black) dashed lines highlight marshes 2 and 3, respectively, while the remaining area represents marsh 1 (this area is highlighted by the thicker lines). The dot shows the location of the CRMS0421

station, and the star indicates the location over the marsh platform where field observations of water levels were collected.

3. Methods

We utilize remotely sensed maps of sub-canopy water-level change to analyze drainage patterns over three marshes in Terrebonne Bay, Louisiana, USA. UAVSAR images were collected in two distinct temporal windows: April 12th 2021 between 19:29 and 22:59 (UTC time), and September 4th 2021 between 16:21 and 20:08 (UTC time). Hydrodynamic conditions are similar during the two campaigns, but vegetation characteristics present marked differences. As such, we can unravel the effect of vegetation on water-level change (WLC) by comparing UAVSAR data measured in the two selected temporal windows.

WLC on marsh platforms is affected by water conveyance. The latter can be expressed by the empirical Manning's formula that applies to uniform flow in open channels:

$$q = \frac{1}{n} \cdot h^{5/3} \cdot i^{1/2} \qquad (1)$$

where *n* is the Manning's roughness coefficient, *h* is the water depth, and *i* represents the water-surface slope. In numerical models, the simplest way to account for the effect of vegetation on a depth-averaged flow is to increase the roughness coefficient with respect to unvegetated areas [e.g., Beudin et al., 2016]. Similarly, model calibration in channels and open water is often performed by varying the roughness coefficient until the simulated water levels match those measured in the field [e.g., Cortese et al., 2023].

To determine the influence of water depth and friction on WLC, we make use of (i) high-spatial resolution topographic data (Figure 2a) [Christensen et al., 2023]; and (ii) two high-spatial resolution maps of herbaceous aboveground biomass (AGB) obtained using AVIRIS-NG hyperspectral imager (see Figure 2b for the AGB distribution during spring) [Jensen et al., 2022]. Note that we employ two AGB maps because the UAVSAR campaigns occurred in two different seasons (i.e., spring and fall, see how vegetation structure changes with seasons in Table 1 [Castañeda & Solohin, 2021]). The intensive site was dominated by *Spartina alterniflo*ra during the spring campaign, and by a mix of *Spartina alterniflo*ra and *Juncus roemerianus* during the March-April campaign (Figure 3).

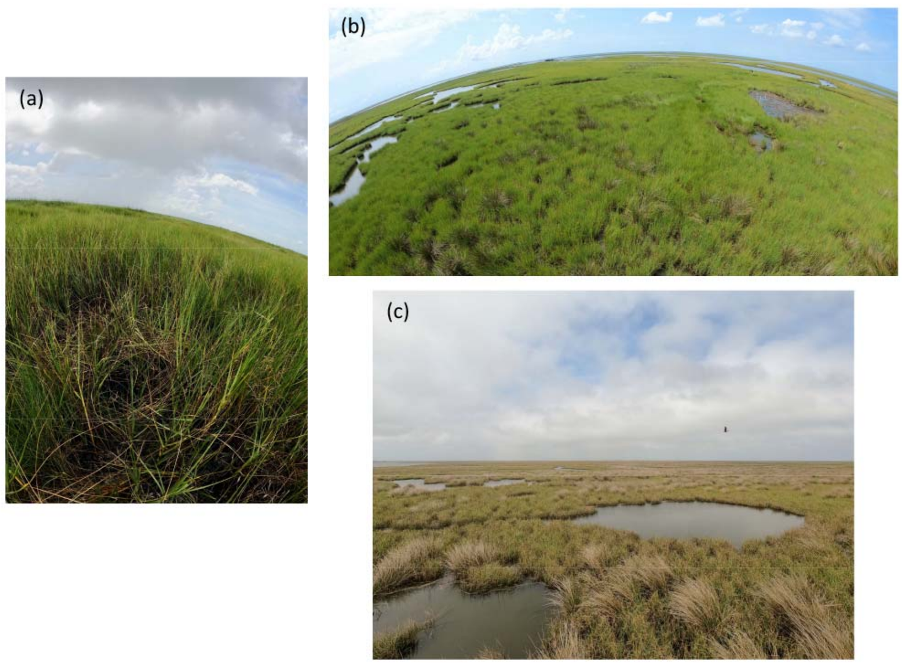

Figure 3. Field images of vegetation types in the (a, b) spring and (c) fall campaigns.

It is important to highlight that part of the measurements collected during the September 4, 2021, UAVSAR flight is affected by atmospheric effects (see Figure S1 and Movie S1 in Supporting Information S1) which prevents the use of these data. This means we cannot use all the data taken in this campaign. More specifically, WLC measured over the largest marsh (marsh 1 in

Figure 2b) is partially corrupted due to variations in atmospheric properties between the different SAR acquisitions [e.g., Hanssen et al., 2001].

The procedure adopted here to analyze the spatial variability in salt marsh drainage can be summarized as follows: (i) we use UAVSAR data (subsection 3.1) and field observations of water level (subsection 3.2) to evaluate whether UAVSAR provides reliable estimations of WLC on marsh surfaces; (ii) we employ the WLC measurements collected during the April 12, 2021, UAVSAR flight to determine whether marshes characterized by the same elevation present comparable changes in water level within the same temporal window; (iii) we utilize the AGB map in spring (subsection 3.3, see Figure 2b) to evaluate the effect of spatial variations in vegetation characteristics on the distribution of WLC; (iv) we use UAVSAR data to understand the role of small features in the marsh landscape (i.e., levees and channels) on water movement; (v) we employ WLC measurements collected during the April 12, 2021, and the September 4, 2021, UAVSAR flights to determine the influence of seasonal changes in AGB on WLC over marshes 2 and 3 (i.e., where UAVSAR data are not affected by atmospheric effects during the September 4, 2021, UAVSAR flight, see Figure 2b).

3.1 UAVSAR interferometry

UAVSAR is a synthetic aperture imaging radar deployed on a Gulfstream-3 aircraft that collects measurements of Earth's surface change from 12.5 km altitude. The instrument is a fully polarimetric (i.e., it transmits horizontal and vertical pulses and receives returns from each in both polarizations), left-looking synthetic aperture radar that operates in L-band (λ= 0.2379 meters of wavelength) with center frequency of 1.2575 GHz and 80 MHz of bandwidth. The radar images a region 22 km wide, with incidence angle ranging between ~22° (near range) to ~67° (far range) [Garcia-Pineda et al., 2013].

A collection of UAVSAR measurements were performed over the entire salt-marsh system in Terrebonne Bay. The region was scanned six times between 19:29 and 22:58 (UTC time) on April 12th, 2021, and between 16:21 and 20:08 (UTC time) on September 4th, 2021. The goal of these measurements is to take advantage of the rapid-repeat pass capability of UAVSAR and capture WLC over flooded surfaces with emergent vegetation. This capability is possible due to the double-bounce radar-pulse return that bounces from both the water surface and the vegetation [Lu & Kwoun, 2008; Dabboor & Brisco, 2018], allowing measurement of WLC in areas with sparse gauge coverage. In particular, we used pairs of rapid-repeat pass SAR acquisitions acquired by UAVSAR to form sets of interferograms employing the InSAR Scientific Computing Environment (ISCE) [Rosen et al. 2000]. We then performed phase unwrapping to quantify the number of 2π cycles, to be able to accurately derive the total displacement in water level. Once the interferograms were unwrapped, we used them to estimate the InSAR derived WLC time series, as described in the product documentation available at the ORNL DAAC (https://daac.ornl.gov/DELTAX/guides/DeltaX_L3_UAVSAR_WaterLevels.html) [Jones et al., 2022]. This method can be similarly applied to different wetland types (e.g., mangroves). However, its effectivity will be highly dependent on the repeat pass schedule of the observing sensor as well as the type of vegetation observed. If the vegetation has a soft stem, its scattering properties will change rapidly and data acquisition will require a very short repeat observation time, whereas woody vegetation may allow for a longer temporal baseline in the SAR acquisition pattern [Oliver-Cabrera et al., 2021]. Note that the method cannot be applied to submerged vegetation, e.g. seagrass.

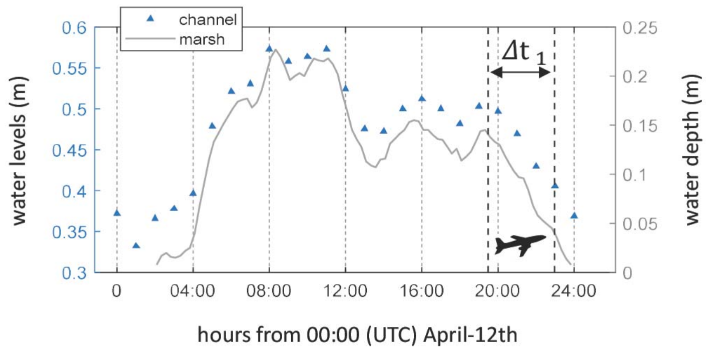

Figure 4. Field measurements of water levels (m) in the channel (triangles, CRMS-421 station, see Figure 2), and water depth over marsh (solid line, lat 29.170201, lon -90.823649, see Figure 2). Water levels are measured with respect to NAVD88. These observations were collected in April 12, 2021. Δt_1 represents the interval of time in which the UAVSAR flight took place.

3.2 Field measurements of water levels

The Coastwide Reference Monitoring System (CRMS) was designed by the Louisiana State Wetlands Authority, and the Coastal Wetlands Planning, Protection, and Restoration Act (CWPPRA) Task Force to evaluate the effectiveness of restoration projects at multiple spatial scales along the Louisiana coastline. Instruments at nearly 400 sites continually monitor soils, hydrology, land change, and vegetation since 2003. These stations provide hourly water-level data, which are used to analyze spatial variations in hydrodynamic conditions at different temporal scales. We employ water-level observations from the CRMS-0421 station (see red dot in Figure 2b) to evaluate how water levels vary in a channel adjacent to the three selected marshes during the UAVSAR flights.

These data are complemented with field measurements of water levels on the neighboring marsh platform (see red star in Figure 2b). The instrument on the marsh was installed at approximately 3 cm above the soil surface (thus we do not have data when water level was lower than 3 cm) and collected water-level data every 20 minutes. Measurements are expressed with respect to NAVD88.

3.3 Above Ground Biomass (AGB)

We utilize two maps of herbaceous aboveground biomass (AGB), derived from Airborne Visible Infrared Imaging Spectrometer-Next Generation (AVIRIS-NG) data, developed by Jensen et al., [2022; 2023] for the spring and fall seasons. AVIRIS-NG is an imaging spectrometer that measures radiance at 5 nm sampling across 425 bands in the Visible to Short-Wave Infrared (VSWIR) spectral range (380-2500 nm). The L1 radiance data were processed to L2 surface reflectance products with atmospheric correction [Thompson et al. 2019], with further corrections applied to adjust for Bidirectional Reflectance Distribution Function (BRDF) effects [Greenberg et al. 2022; Thompson et al. 2022]. AGB, quantified as dry biomass in grams per square meter (g/m^2), was estimated from the BRDF-adjusted surface reflectance and a coincident AGB field survey [Castañeda-Moya & Solohin 2022]. A machine learning model was generated to estimate AGB by comparing local pixel reflectance spectra with coincident in-situ samples of herbaceous vegetation AGB. This model ($R^2 = 0.89$, Mean Absolute Error = 109.30 g/m^2) was then scaled to the AVIRIS-NG mosaic imagery to map herbaceous AGB across the Terrebonne Basin. The instrument is also used to measure water quality and suspended sediment concentration in coastal regions [e.g., Jensen et al., 2019]. The map has a spatial resolution of ~5 m. The AGB map is depicted in Figure 2b. A detailed description of how the AGB map was obtained is reported in Jensen et al. [2022].

4. Results

Field measurements of water levels show that the tidal signal in the channel and over the marsh are generally in phase (Figure 4). However, a small phase shift between these two signals may exist and be spatially variable, and it depends on the distance between the channel and the location where water levels are measured over the marsh. We use data from UAVSAR to analyze the spatial variability in WLC over the selected marshes (Figure 2b). The maps representing WLC on marsh platforms are shown in Figure S2 for the April 12, 2021, UAVSAR flight (see Supporting Information S1); the temporal window (Δt_1) in which the UAVSAR campaign took place is shown in Figure 4. UAVSAR-derived WLC in the marsh pixels located next to the CRMS station 0421 matches well the field measurements.

Since WLC on marsh platforms depends on flow conveyance, we plot UAVSAR-derived WLC as a function of marsh elevation (see subsection 4.1) and AGB (see subsection 4.2). Then we select various marsh sub-regions and we focus on the presence of small geomorphic features (width smaller than 10 meters) in the marsh landscape. Such geomorphic features may affect water transport in marshes, and consequently WLC on platforms (see subsection 4.3). In the same subsection, we also evaluate the effect of seasonal changes in vegetation characteristics on WLC.

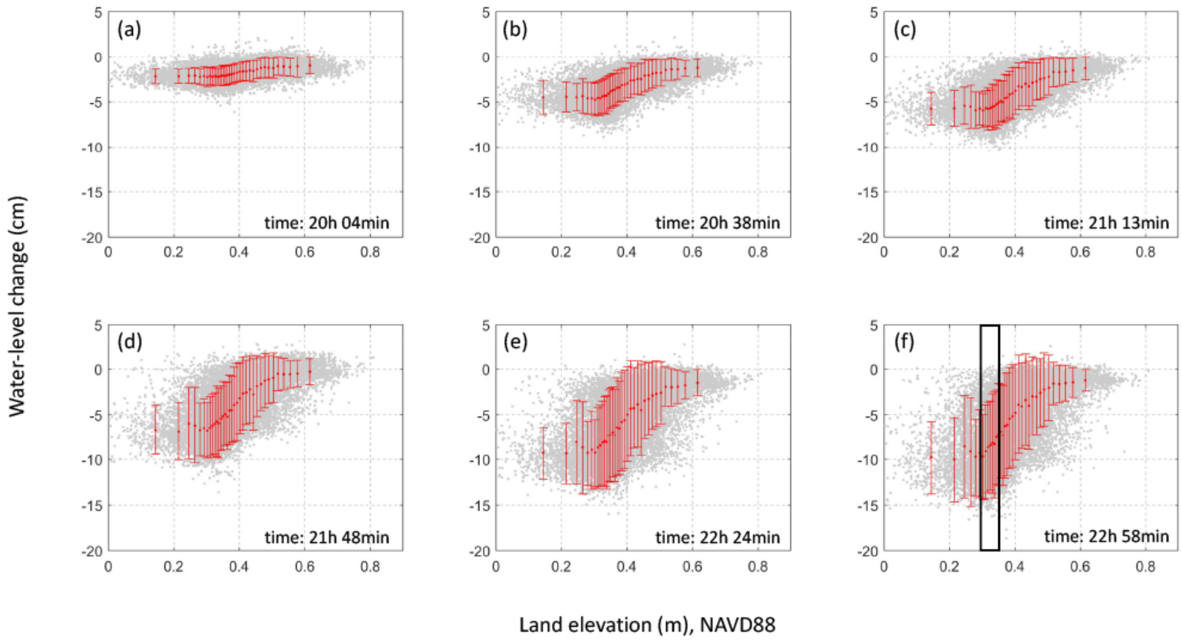

Figure 5. UAVSAR-derived WLC (cm) as a function of marsh elevation (m) for different intervals of time, starting at t = 19:29 UTC and ending at the time indicated on each plot. Red dots represent median values and the red bars indicate the interquartile range. WLC was measured during the April 12, 2021, UAVSAR flight. The rectangle in Figure 5f shows the interval of marsh elevation that is considered in Figure 6.

4.1 WLC as a function of marsh elevation

We plot WLC estimated during the April 12, 2021, UAVSAR flight as a function of marsh height (Figure 5). The values are change in water level relative to the first acquisition, which was made at 19:29 UTC. Our aim is to determine if vegetated pixels (hereinafter called also marsh pixels) characterized by the same elevation within the local tidal range experience a similar change in water level over the selected temporal window (Figure 5). We modified the spatial resolution of the UAVSAR data (and later that of AVIRIS-NG, see subsection 4.2) to obtain the same resolution of the available bathymetry (i.e., 10m). In particular, we resampled the raster to a lower resolution by using a standard method for resampling (i.e., nearest neighbor). Figure 5 depicts WLC as a function of marsh height in six different temporal windows (these six temporal windows start at 19:29, and end at 20:04, 20:38, 21:13, 21:48, 22:24 and 22:58 respectively). Note that WLC increases in absolute value with respect to the first UAVSAR acquisition. Interestingly, vegetated pixels with a similar elevation can exhibit a different change in water level, indicating that water can drain differently from locations of similar elevation, depending on their location within the marsh. This result is highlighted by the interquartile range in UAVSAR-derived WLC which varies as a function of marsh elevation (Figure 5).

The substantial variability in WLC showed by marsh pixels located at the same elevation can potentially be related to spatial variations in vegetation characteristics. We investigate the relationship between change in water level and above ground biomass in the next subsection.

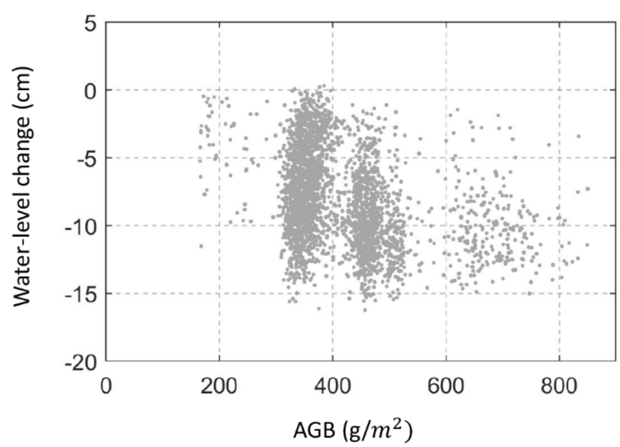

Figure 6. UAVSAR-derived WLC (cm) as a function of AGB (g/cm^2). WLC was measured during the April 12, 2021, UAVSAR flight during the time interval 19:29 - 22:58 UTC. We only consider marsh pixels with an elevation between 0.3 and 0.35 meters (see rectangle in Figure 5f).

4.2 Effect of vegetation on the distribution of WLC

We utilize the map of AGB in the spring (Figure 2b) to determine the effect of vegetation on WLC during the April 12, 2021 UAVSAR flight. We only consider marsh pixels with an elevation between 0.3 and 0.35 meters (since the majority of vegetated pixels in the selected group of marshes have an elevation within this range). In other words, we fix marsh height (see rectangle in Figure 5f) to evaluate the relationship between WLC and AGB. When WLC is plotted as a function of the above ground biomass (Figure 6) the results reveal a weak correlation between these two variables. Surprisingly, changes in water level (in absolute value) within the selected temporal window of 3.5 hours seem to increase with greater values of above ground biomass.

It should be noted that WLC measured by UAVSAR occurs only in the portion of the water column occupied by plants. This can be easily verified by comparing field measurements of water level over the marsh (Figure 4) with the data of vegetation structure collected between March 21, 2021 and March 31, 2021 (Table 1). The maximum water level observed over the marsh during the selected temporal window is 15 cm, which is indeed smaller than the plant height reported in Table 1.

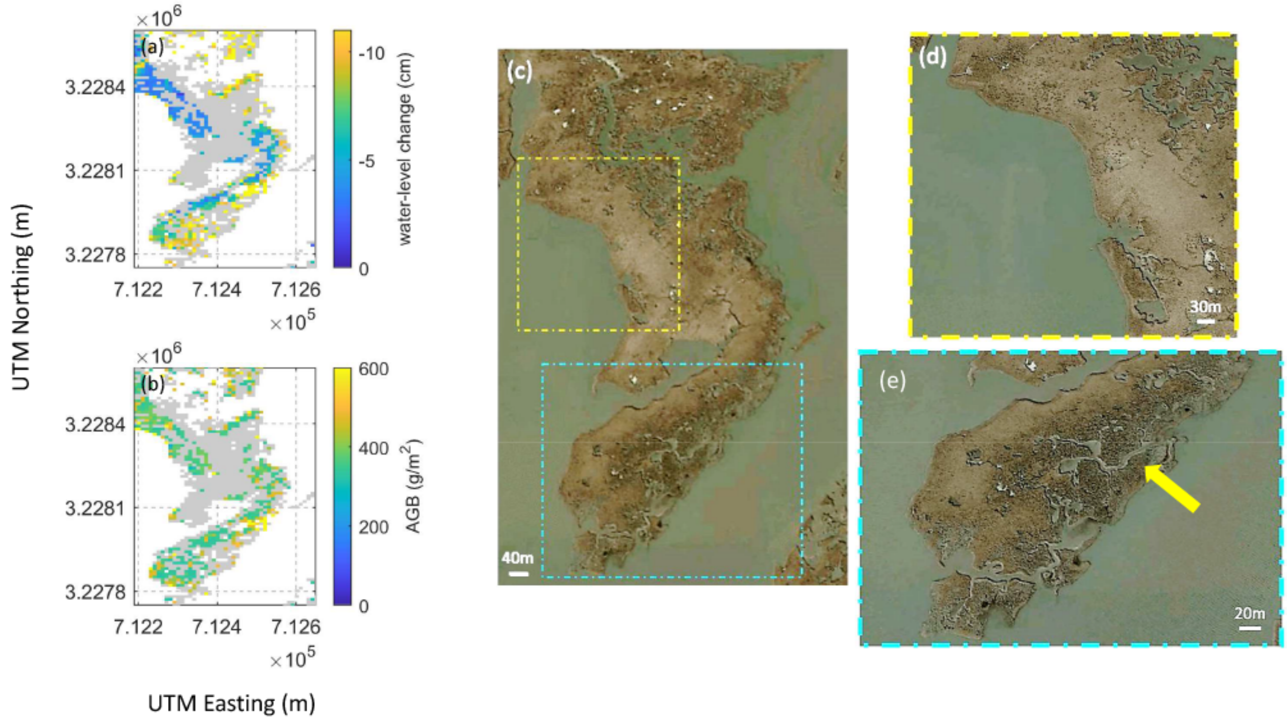

Figure 7. Spatial distribution of (a) UAVSAR-derived WLC (cm), and (b) AGB (g/m^2) values in spring for a sub-region of marsh 1. WLC was measured during the April 12, 2021, UAVSAR flight. Satellite images: (c) entire sub-region; (d) and (e) close up of two different parts of the selected sub-region (i.e., area without channels and highly channelized area). The arrow indicates the presence of small tidal channels with a width of 2 and 5 meters. (image ©Google, Landsat/Copernicus).

4.3 Effect of small geomorphic features in marsh landscape on WLC

We analyze images from satellite (Google Earth) to identify the presence of small geomorphic features in the marsh landscape. Such elements may affect water conveyance on marsh platforms, allowing for more or less tidal propagation within surrounding areas. First, we map the spatial distribution of WLC and AGB within the selected sub-regions. Then, we utilize images from satellite to understand why pixels with a similar elevation drain water differently.

We start by considering the sub-region depicted in Figure 7 (this sub-region is part of marsh 1 depicted in Figure 2b). Here, we show the spatial distribution of (i) WLC measured during the April 12, 2021, UAVSAR campaign (Figure 7a), and (ii) AGB values during the spring (Figure 7b). We only focus on pixels with an elevation between 0.3 and 0.35 meters. These pixels present a substantial variability in WLC with values ranging between 0 and 11 cm (Figure 7a).

We show images of this sub-region in Figure 7c, d, e. These images reveal that the vegetated pixels exhibiting larger values of WLC are located next to tidal channels which are not captured by the available bathymetric data (see the arrow in Figure 7e). Such channels (width ranging between 1 meter and 10 meters) help drain water from the marsh surface, therefore increasing WLC within the adjacent vegetated pixels (see Figure 7e).

We apply the same approach to marshes 2 and 3 (see Figure 2b). UAVSAR data from another campaign are also available for these marshes. Figure 8 shows water levels measured at the CRMS-0421 station in the channel and over the marsh for September 4, 2021. In the same figure, we show the temporal window in which the UAVSAR flight took place (Δt_2).

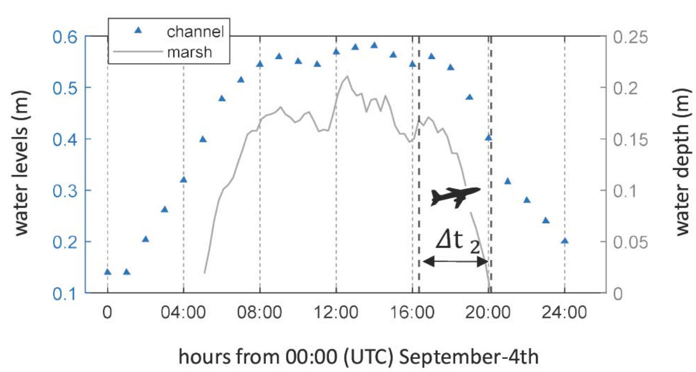

Figure 8. Field measurements of water levels (m) (i) in the channel (CRMS-421 station), and (ii) over the marsh (lat 29.170201, lon -90.823649). Water levels are measured with respect to NAVD88. These observations were collected in September 4, 2021. Δt_2 represents the interval of time in which the UAVSAR flight took place.

Histograms of WLC and AGB are reported in Figure 9. Table 2 lists the mean, median, standard deviation, interquartile range, and skewness for each distribution. Here, we use the median as a measure of the typical value of WLC. Note that the typical value is greater for the September 4, 2021, UAVSAR campaign compared to the April 12, 2021, UAVSAR campaign. This result is consistent with field observations of water level collected over the marsh (Figures 4-8).

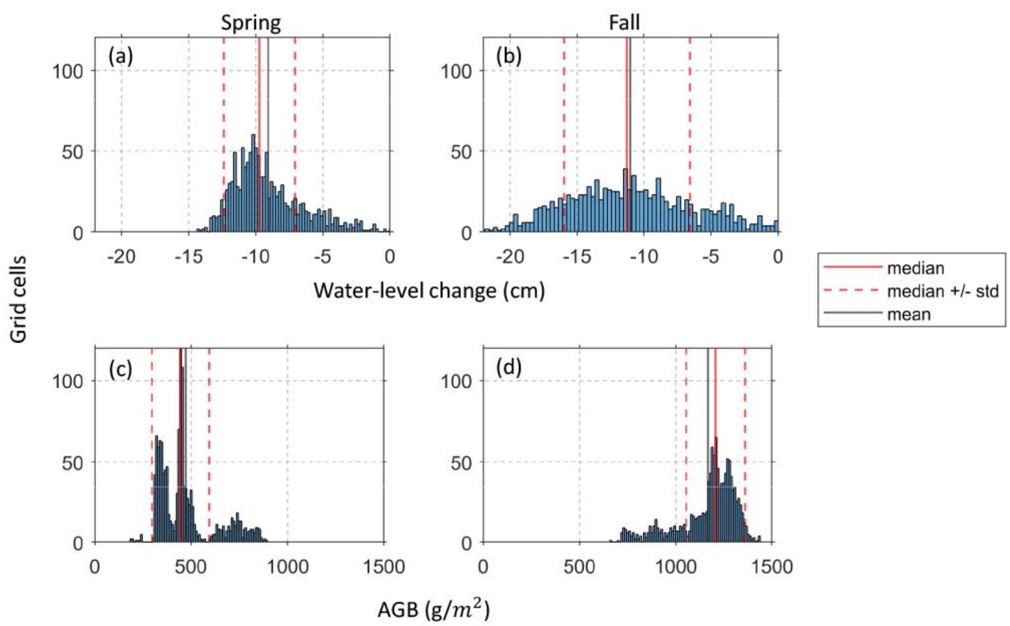

Figure 9. Histograms of (a, b) WLC and (c, d) AGB for marsh 2 (see Figure 2b) during (a, c) the April 12, 2021, and (b, d) September 4, 2021, UAVSAR flights. The solid red line represents the median value, while the dashed lines represent the median value plus/minus one standard deviation. The black line represents the mean value. WLC is considered positive if it corresponds to an increase of water level in the selected temporal window.

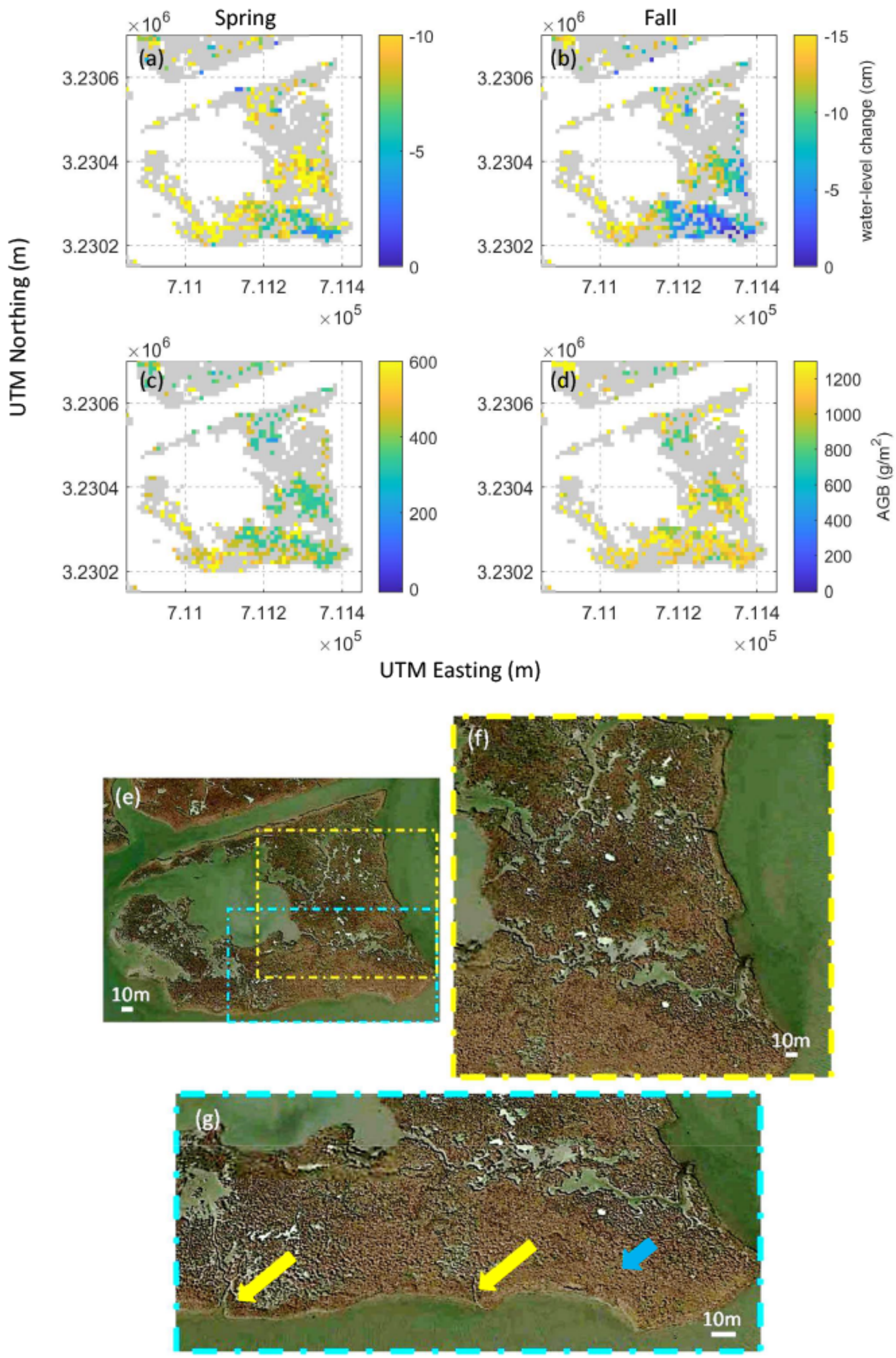

Figure 10. Spatial distribution of (a, b) UAVSAR-derived WLC (cm), and (c, d) AGB (g/m^2) values in spring (a, c) and fall (b, d) for marsh 2. WLC was measured during the April 12, 2021, and September 4, 2021, UAVSAR flights. Satellite images: (e) entire marsh 2; (f) and (g) close up of two different parts of the selected marsh. Images (f) and (g) highlight the presence of small tidal channels in the marsh landscape. The large (yellow) arrows highlight the presence of two small tidal channels with a width of 2-3 meters. The small (blue) arrow indicates an area of the marsh where tidal channels are absent. (image ©Google, Landsat/Copernicus).

Spatial distributions of WLC and AGB for marsh 2 are shown in Figure 10. We only consider pixels with an elevation between 0.35 and 0.40 meters (since the majority of pixels in marsh 2 have an elevation within this range). WLC (Figure 10a, b) within the two selected temporal windows presents a similar spatial distribution (R=0.64). By contrast, the AGB maps do not exhibit a similar spatial pattern between spring and fall (R=-0.22). This result implies that, despite both the substantial increase in AGB values (see histograms in Figure 9c, d) and the occurrence of marked changes in their spatial distribution, WLC remains fairly similar within the two UAVSAR campaigns. By using satellite images (Figure 10e, f, g), we observe that the area of the marsh experiencing greater changes in water level (Figure 10a, b) is fragmented (see Figure 10f, g; the large arrows in Figure 10g highlight the presence of two small tidal channels). In contrast, the WLC is lower where tidal channels are absent (see for instance the marsh area highlighted by the small arrow in Figure 10g).

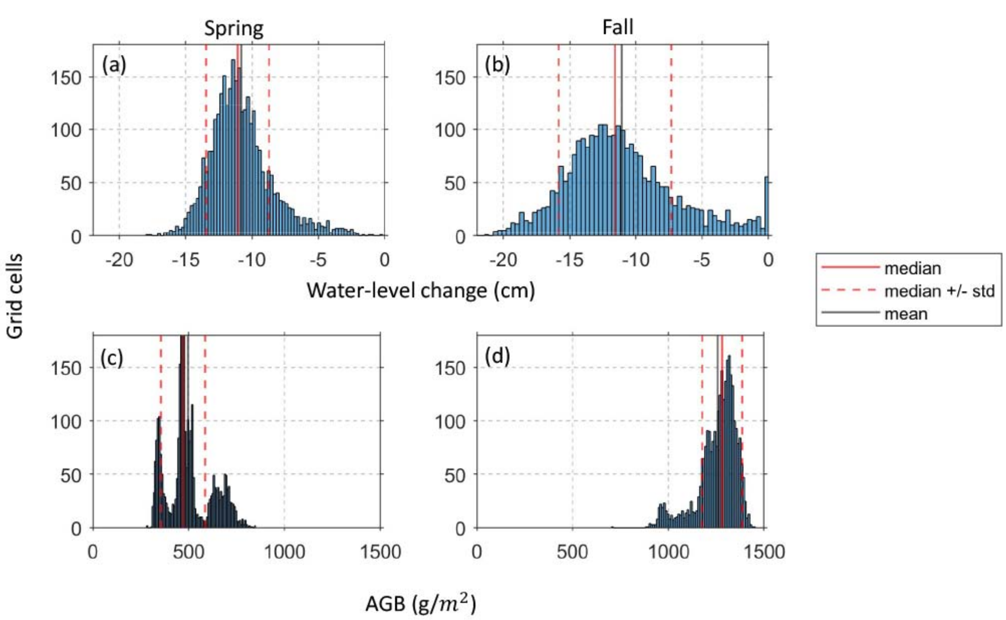

Figure 11. Histograms of (a, b) WLC and (c, d) AGB for marsh 3 (see Figure 2b) during (a, c) the April 12, 2021, and (b, d) September 4, 2021, UAVSAR flights. The solid red line represents the median value, while the dashed lines represent the median value plus/minus one standard

deviation. The black line represents the mean value. WLC is considered positive if it corresponds to an increase of water level in the selected temporal window.

Finally, we focus on the third marsh. Histograms of WLC and AGB highlight differences between the two selected temporal windows (Figure 11). Table 3 shows the mean, median, standard deviation, interquartile range, and skewness for each distribution. We plot maps of WLC and AGB in spring and fall (Figure 12). Note that a low correlation exists between the two maps of WLC (R=0.33), and between the maps of AGB (R=-0.21). By comparing Figures 12a, b with satellite images (Figure 13), we observe that levees are present where WLC is much lower compared to the median value (see for instance the arrow in Figure 13b). Furthermore, we note that this marsh is highly fragmented (Figure 13c), and, as such, it exhibits a smaller standard deviation of WLC compared to marsh 2 (see Tables 2-3).

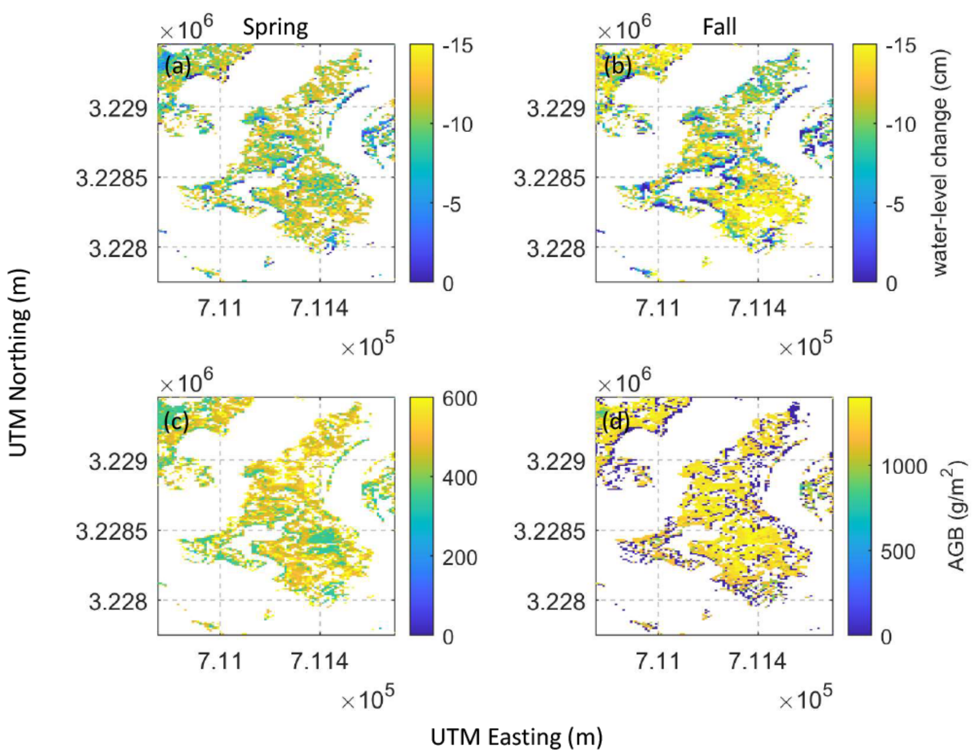

Figure 12. Spatial distribution of (a, b) UAVSAR-derived WLC (cm), and (c, d) AGB (g/m^2) values in spring (a, c) and fall (b, d) for marsh 3. WLC was measured during the April 12, 2021 and September 4, 2021 UAVSAR flights.

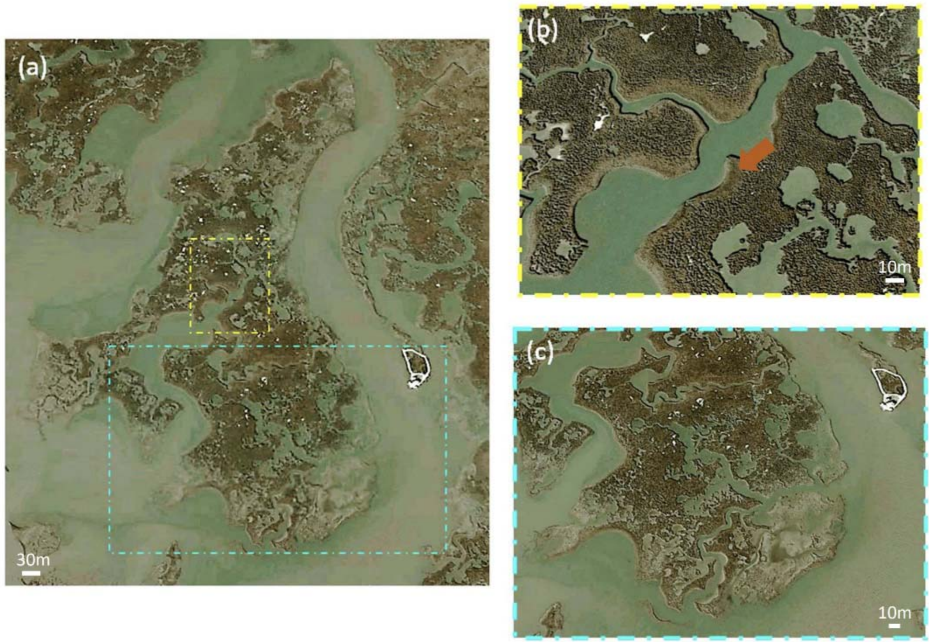

Figure 13. Satellite images: (a) entire marsh 3; (b) and (c) close up of two different parts of the selected marsh. Image (b) highlights the presence of levees, whereas image (c) shows a sub-region of marsh 3 which is highly channelized. The arrow indicates the presence of levees. (image ©Google, Landsat/Copernicus).

5. Discussion

We utilized a new generation of remotely sensed data to study the interactions of vegetation, topography, and flow on marsh platforms. These interactions have been explored for three salt marshes located in Terrebonne Bay, Louisiana (see Figures 1-2). In particular, we focused on unravelling what factors influence spatial variations in WLC on marsh platforms at hourly time scales. To this end we used (i) multiple images of UAVSAR-derived WLC collected during falling tides, (ii) bathymetric data from lidar, and (iii) high-spatial resolution maps of AGB obtained through AVIRIS-NG.

5.1 WLC as a function of marsh topography

Our results reveal that marsh platforms exhibit a substantial spatial variability in WLC (e.g., Figure 5). Interestingly, marsh pixels characterized by the same elevation within the local tidal range present marked differences in WLC. Part of this variability can be explained by the presence of errors in the lidar data. In particular, the laser cannot penetrate into thick vegetation canopies leading to a positive bias in bed elevation. Such bias is spatially variable and depends on vegetation density [e.g., Medeiros et al., 2015; Rogers et al., 2018; Cooper et al., 2019]. This result means we cannot correct topographic errors by uniformly lowering the bathymetry, but an ad-hoc change in bed elevation is needed for each point of the domain.

Zhang et al. [2022a; b] proposed to correct wetland bathymetry (i.e., remove the positive bias) by employing data from UAVSAR and numerical modelling. However, it turned out in their study that the derived topographic corrections were either positive or negative (i.e., bed elevations were also biased towards a lower elevation). Since the bias in bathymetric information due to the laser's inability to penetrate vegetation can be only positive, it is likely that the negative bias can be related to the presence of geomorphic elements in the marsh that are not captured in the model grid [e.g., Blanton et al., 2010]. These topographic features (e.g., small levees) promote water retention within the surrounding vegetated areas, leading to a smaller WLC.

It is worth noting that the empirical/iterative approach of Zhang et al. [2022a; b] could modify bed elevations even in regions where corrections are not needed. If the spatial resolution of the model is too coarse to capture the presence of small tidal creeks (note that tidal creeks facilitate water drainage on marsh surface and therefore increase WLC), a decrease in bed elevation and/or friction would be required. Specifically, these modifications would increase water conveyance on platforms, and consequently augment the change in water level within the selected temporal window. On the other hand, corrections in bathymetry and/or friction would not only alter local hydrodynamics (i.e., where changes are made) but they would also propagate to areas downstream leading to an overall decrease of model accuracy in reproducing WLC within vegetated areas. As such, it is essential that topographic data have sufficient spatial resolution to identify small tidal creeks and levees on marsh platforms, e.g., 1-meter spatial resolution. This condition is important to (i) capture the enormous spatial variability in hydrodynamic conditions across marsh landscapes via numerical modeling; (ii) minimize possible fictitious changes in bed elevation and/or friction introduced by the procedure proposed by Zhang et al., [2022a; b]; and (iii) remove the effects related to errors in topography.

5.2 Effect of vegetation on WLC

The interaction between flow and vegetation is complex and has been explored at different spatial and temporal scales [e.g., Liu et al., 2003; Mazda et al., 1997; Temmerman et al., 2005; Wu et al., 2001; Donatelli et al., 2019]. Until now, we did not have observations that provide a spatially-continuous view of how tides propagate in wetlands. UAVSAR repeat-pass interferometry provides, for the first time, a synoptic view of WLC across vegetated areas. This remote sensing technique allows us to study the hydrodynamics in these ecosystems at an unprecedented spatial resolution.

Water retention on marsh platforms depends on (i) the degree of channelization, which affects the transport of water from marsh interior towards the surrounding environment; (ii) levees, which obstruct the flow and do not allow the water to drain following the shortest and steepest path, and (iii) vegetation, which exerts a drag on the flow and thus slows down tidal currents. In this study, we show that WLC on marshes during falling tides is not affected by spatial and temporal changes in AGB (e.g., Figure 6). This finding is a counterintuitive one, since it is well known that vegetation increases friction on tidal currents [e.g., Gerkema, 2019] and alters spatial flow patterns in tidal landscapes [e.g., Temmerman et al., 2007; 2012]. However, we argue that in highly channelized marshes, such as those in Terrebonne Bay, the ebb flow is preferentially transported via channels. Therefore, vegetation has a limited effect in retaining water on marsh surfaces. This result is broadly consistent with Montgomery et al. [2018] and Pelckmans et al. [2023], who found a similar behavior in mangroves. They both showed that vegetation attenuates long waves only if the transport of water through the vegetation is the main mechanism of fluid transport. If creek flow dominates, the density of mangrove vegetation has a minimal effect on the attenuation of water levels [e.g., Horstman et al., 2015]. Our finding also agrees with Zhang et al. [2022a] who showed through numerical modelling that large variations in friction on marsh platforms have a minimal impact on WLC.

Another factor that could diminish the effect of vegetation on WLC is water depth. When vegetation is fully submerged and occupies only part of the water column, large-scale sheet flow (i.e., flow above the canopy) becomes important and relative spatial differences in friction decrease [Temmerman et al., 2005; Fagherazzi et al., 2012; Nepf, 2012]. The two 3.5-hour UAVSAR campaigns were conducted during falling tides with an initial water level in the channel of ~0.5 meters (Figures 4-8). By comparing water levels on the marsh with plant height (Table 1), we deduce that WLC occurs in the part of the water column occupied by plants. Therefore, the transport of water did not occur through sheet flow during the selected temporal windows and tidal conditions.

5.3 Temporal variability in hydrodynamic conditions

Water movement in wetlands depends on two major drivers, namely tides and wind. While the former has a cyclical character, the latter is episodic in nature and can even vary from year to year [e.g., Donatelli et al., 2022a; b]. WLC on marshes may differ due to tidal variations (e.g., spring-neap modulation), freshwater discharge, wind speed and direction, and duration of wind events [e.g., Gerkema & Duran-Matute, 2017; Valentine & Mariotti, 2018]. Obviously, this type of UAVSAR flight campaign with repeated imaging within a single flight cannot reveal changes across the range of time scales. This remote sensing technique can only provide multiple images of WLC beneath the vegetation canopy within a short temporal window (i.e., it offers hydrodynamic information at an hourly time scale).

As documented by previous studies, meteorological events have a paramount effect on water levels in Terrebonne Bay [e.g., Reed, 1989], implying that WLC on marsh platforms can strongly deviate from its long-term statistics (i.e., long-term mean and/or median). In other words, the WLC measured by the two UAVSAR campaigns might not be representative of the typical hydrodynamic conditions experienced by salt marshes during ebb tide. To explore the temporal variability of such changes in water level at short- and long-time scales, a combination of UAVSAR images and numerical modeling is needed [e.g., Zhang et al., 2022a; b]. This task is not trivial, especially if we want to investigate marsh hydrodynamics at a very high spatial resolution, which this study indicates is important, and at the same time employ numerical simulations spanning several years [e.g., Donatelli et al., 2022b]. In fact, a grid size of ~1 meter would dramatically increase the simulation time and consequently reduce the performance of the model, while a model with a larger resolution (e.g., 10 meters) would not be able to consider the effect of levees and small channel on WLC within vegetated areas.

5.4 Implications for coastal vulnerability predictions

This new generation of remotely sensed data can also be used to achieve a precise estimation of fluxes of water and its constituents in coastal environments, which is essential to evaluate the impact of climate change on wetlands. A robust quantification of such fluxes allows us to predict which parts of a salt-marsh system will erode and which parts will grow; this information can be employed, for instance, to design effective interventions along the shoreline, and forecast the location and timing of new land creation through sediment accumulation [e.g., Winterwerp et al., 2020; Tas et al., 2022]. Additionally, UAVSAR observations may be applied to improve the accuracy of numerical models to simulate hydrodynamics within vegetated areas, which is fundamental to quantify the impact of future extreme events on coastal communities [e.g., Aretxabaleta et al., 2019; Temmerman et al., 2022]. A better understanding of how water levels are impacted by vegetation is important to limit the economic impact of coastal hazards, and increase the capability of communities and coastal economies to recover [e.g., Goreau & Hilbertz, 2005].

6. Conclusions

The main conclusions of this paper can be summarized as follows:

1. UAVSAR can measure changes in water level across salt marshes at an unprecedented spatial resolution. These data prove reliable in capturing the effect of small geomorphic features (width smaller than 10 meters) on WLC within these vegetated environments.
2. We utilized UAVSAR data to investigate drainage patterns over three salt marshes in Terrebonne Bay, USA. Our study shows that these marshes exhibit substantial variability in WLC during falling tides.

3. Small tidal channels and levees affect WLC on marsh surfaces. More specifically, these geomorphic elements affect water transport within the adjacent vegetated areas and, as a consequence, influence WLC. This finding explains why portions of a marsh characterized by the same elevation can drain water differently.
4. The presence of small channels in marshes can be easily detected via UAVSAR by mapping the spatial distribution of WLC.
5. Vegetation has a minimal effect on water retention in the selected marshes. Our result suggests that in highly-channelized marshes, spatial and seasonal changes in AGB do not have a substantial influence on WLC. This result implies that water transport during ebb tides occurs mainly through channels, and, as such, vegetation has a small influence in retaining water on platforms.

Acknowledgments

We thank the Editor, the Associate Editor, and the three anonymous Reviewers for their comments. Dr. Elena Solohin and Dr. Edward Castaneda provided field data and pictures of vegetation characteristics. This work within the NASA Delta-X project is funded by the Science Mission Directorate's Earth Science Division through the Earth Venture Suborbital-3 Program NNH17ZDA001N-EVS3. This work was partly performed by the Jet Propulsion Laboratory, California Institute of Technology, under contract with the National Aeronautics and Space Administration (NASA). S.F. was also funded by NASA Earth System Science for Building Coastal Resilience award 80NSSC23K0129, NSF grants DEB-1832221 to the Virginia Coast Reserve Long-Term Ecological Research project and OCE- 2224608 to the Plum Island Ecosystems Long- Term Ecological Research project.

Open research

The data of aboveground biomass (AGB) from AVIRIS-NG can be accessed through the ORNL DAAC, which is open for public access and download (Jensen et al., 2021): https://doi.org/10.3334/ORNLDAAC/1822. The data of water-level change (WLC) from UAVSAR can be accessed and downloaded through the ORNL DAAC (Jones et al., 2022): https://doi.org/10.3334/ORNLDAAC/2058. The digital elevation model (DEM) can be accessed and downloaded through the ORNL DAAC (Christensen et al., 2023): https://doi.org/10.3334/ORNLDAAC/2181.

Supplementary material: figure captions

Figure S1. (a, b, c, d, e, f) Time series of WLC show a pattern that does not seem to follow the expected water levels. Yellow indicates an upwards change through the previous steps. (h) When compared against a nearby station CRMS0307, the discrepancy between inSAR and water level can be observed. (i) Weather radar image of the area at the time 17:23 from the KLIX station located in New Orleans reveals atmospheric patterns spread through the region. Note that weather radar shows reflectivity of 8 db and above. WLC was measured during the September 4, 2021, UAVSAR flight.

Figure S2. Maps of UAVSAR-derived WLC for different intervals of time. WLC was measured during the April 12, 2021, UAVSAR flights.

Movie S1. Animation of WLC. Yellow indicates an upwards change through the previous steps. The study site is located towards the lower center. WLC was measured during the September 4, 2021, UAVSAR flight.

References

Alsdorf, D.E., Rodriguez, E., Lettenmaier, D.P., (2007). Measuring surface water from space. Rev. Geophys. 45, RG2002.

Aretxabaleta, A.L., Ganju, N.K., Defne, Z., and Signell, R.P., (2019). Spatial distribution of water level impacting back-barrier bays, Nat. Hazards Earth Syst. Sci., 19, 1823–1838, https://doi.org/10.5194/nhess-19-1823-2019.

Ayoub, F., Jones, C. E., Lamb, M. P., Holt, B., Shaw, J. B., Mohrig, D., & Wagner, W. (2018). Inferring surface currents within submerged, vegetated deltaic islands and wetlands from multi-pass airborne SAR. Remote Sensing of Environment, 212, 148–160. https://doi.org/10.1016/j.rse.2018.04.035

Beudin, A., Kalra, T. S., Ganju, N. K., & Warner, J. C., (2017), Development of a coupled wave-flow vegetation interaction model. Computers & Geosciences, 100, 76–86

Blanton, J.O., Garrett, A.J., Bollinger, J.S., Hayes, D.W., Koffman, L.D., Amft, J., & Morre, T. (2010), Transport and retention of aconservative tracer in an isolated creek-marsh system.Estuarine, Coastal and Shelf Science, 87(2), 333–345. https://doi.org/10.1016/j.ecss.2010.01.010

Carniello, L., D’Alpaos, A., & Defina, A. (2011). Modeling wind waves and tidal flows in shallow micro-tidal basins. Estuarine, Coastal and Shelf Science, 92(2), 263–276. https://doi.org/10.1016/j.ecss.2011.01.001

Castañeda-Moya, E., & Solohin, E., (2021). Delta-X: Aboveground Vegetation Structure for Herbaceous Wetlands across MRD, LA, USA. ORNL DAAC, Oak Ridge, Tennessee, USA. https://doi.org/10.3334/ORNLDAAC/1997

Cathcart, C., Shaw, J., & Amos, M. (2020). Validation of streaklines as recorders of synoptic flow direction in a deltaic setting. Remote Sensing, 12(1), 148. https://doi.org/10.3390/rs12010148

Christensen, A.L., Denbina, M.W., and Simard, M., (2023). Delta-X: Digital Elevation Model, MRD, LA, USA, 2021. ORNL DAAC, Oak Ridge, Tennessee, USA. [Dataset]. https://doi.org/10.3334/ORNLDAAC/2181

Cooper, H.M., Zhang, C., Davis, S.E., Troxler, T.G., (2019). Object-based correction of LiDAR DEMs using RTK-GPS data and machine learning modeling in the coastal Everglades. Environ. Model. Software 112, 179–191. https://doi.org/10.1016/j. envsoft.2018.11.003

Cortese, L., Donatelli, C., Zhang, X., Nghiem, J.A., Simard, M., Jones, C.E., Denbina, M., Fichot, C.,G., Harringmeyer, J.P., and Fagherazzi, S., (2023). Coupling numerical models of deltaic wetlands with AirSWOT, UAVSAR, and AVIRIS-NG remote sensing data, Biogeosciences Discuss. [preprint], https://doi.org/10.5194/bg-2023-108, in review.

Cortese, L., Fagherazzi, S., (2022). Fetch and distance from the bay control accretion and erosion patterns in Terrebonne marshes (Louisiana, USA). Earth Surf. Process. Landf. 47 (6), 1455–1465

Costanza, R., et al. (2014). Changes in the global value of ecosystem services. Glob. Environ. Change 26, 152–158

Costanza, R., deGroot, R., Braat, L., Kubiszewski, I., Fioramonti, L., Sutton, P., Farber, S., Grasso, M., (2017). Twenty years of ecosystem services: how far have we come and how far do we still need to go? Ecosyst. Serv., 28, pp. 1-16

Dabboor, M., & Brisco, B. (2018). Wetland Monitoring Using Synthetic Aperture Radar Imagery. In D. Gökçe (Ed.), Wetlands Management-Assessing Risk and Sustainable Solutions (pp. 61–84). IntechOpen. https://doi.org/10.5772/32009

Donatelli, C., Ganju, N.K., Kalra, T., Fagherazzi, S., Leonardi, N., (2019), Changes in hydrodynamics and wave energy as a result of seagrass decline along the shoreline of a microtidal back-barrier estuary, Advances in Water Resources, doi: 10.1016/j.advwatres.2019.04.017

Donatelli, C., Duran-Matute, M., Gräwe, U., Gerkema, T., (2022a), Residual circulation and freshwater retention within an event-driven system of intertidal basins, Journal of Sea Research, https://doi.org/10.1016/j.seares.2022.102242

Donatelli, C., Duran-Matute, M., Gräwe, U., Gerkema, T., (2022b), Statistical detection of spatio-temporal patterns in the salinity field within an inter-tidal basin, Estuaries and Coasts, https://doi.org/10.1007/s12237-022-01089-3

Donatelli, C., Passalacqua, P., Wright, K., Salter, G., Lamb, M.P., Jensen, D., Fagherazzi, S., (2023), Quantifying flow velocities in river deltas via remotely sensed suspended sediment concentration, Geophysical Research Letters, 10.1029/2022GL101392

Duran-Matute, M., Gerkema, T., and Sassi, M.G., (2016), Quantifying the residual volume transport through a multiple-inlet system in response to wind forcing: The case of the western Dutch Wadden Sea, J. Geophys. Res. Oceans, 121, 8888–8903, doi:10.1002/ 2016JC011807

Fagherazzi, S., Hannion, M. and D'Odorico, P., (2008). Geomorphic structure of tidal hydrodynamics in salt marsh creeks. Water resources research, 44(2), W02419, doi:10.1029/2007WR006289

Fagherazzi, S., Kirwan, M. L., Mudd, S. M., Guntenspergen, G. R., Temmerman, S., D'Alpaos, A., et al., (2012), Numerical models of salt marsh evolution: Ecological, geomorphic, and climatic factors. Reviews of Geophysics, 50, RG1002. https://doi.org/10.1029/2011RG000359

Fore, A.G., Chapman, B.D., Hawkins, B.P., Hensley, S., Jones, C.E., Michel, T.R., Muellerschoen, R.J., (2015), UAVSAR polarimetric calibration. IEEE Trans. Geosci. Remote Sens. 53 (6), 3481–3491. https://doi.org/10.1109/TGRS.2014.2377637.

French, J.R., Spencer, T., (1993). Dynamics of sedimentation in a tide-dominated back-barrier salt marsh, Norfolk, UK. Marine Geology 110, 315-331

Ganju, N.K., Nidzieko, N.J., and Kirwan, M.L., (2013), Inferring tidal wetland stability from channel sediment fluxes: Observations and a conceptual model: Journal of Geophysical Research: Earth Surface, v. 118, p. 2045–2058, https://doi .org/10.1002/jgrf.20143.

Ganju, N.K., Defne, Z., Kirwan, M.L., Fagherazzi, S., D'Alpaos, A., and Carniello, L., (2017), Spatially integrative metrics reveal hidden vulnerability of microtidal salt marshes: Nature Communications, v. 8, 14156, https://doi.org/10.1038/ ncomms14156

Garcia-Pineda, O., MacDonald, I., Hu, C., Svejkovsky, J., Hess, M., Dukhovskoy, D., S.L., M., (2013). Detection of floating oil anomalies from the Deepwater Horizon oil spill with synthetic aperture radar. Oceanography 26, 124–137

Gerkema, T., (2019), An Introduction to Tides: Cambridge, UK, Cambridge University Press, 214 p., https://doi.org/10.1017/9781316998793

Goreau, T., Hilbertz, W., (2005). Marine ecosystem restoration: costs and benefits for coral reefs. World Res Rev. 17(3):375–409.

Greenberg, E., Thompson, D.R., Jensen, D., Townsend, P.A., Queally, N., Chlus, A., Fichot, C.G., Harringmeyer, J.P., and Simard, M., (2022). An improved scheme for correcting remote spectral surface reflectance simultaneously for terrestrial BRDF and water-surface sunglint in coastal environments. Journal of Geophysical Research: Biogeosciences 127:e2021JG006712. https://doi.org/10.1029/2021JG006712

Hanssen, R.F., (2001). Remote Sensing and Digital Image Processing, in: van der Meer, F. (Ed.), Radar Interferometry: Data interpretation and error analysis. Kluwer Academic Plublishers, Dordrecht, The Netherlands. volume 2 of Earth and Environmental Science

Hensley, S., Wheeler, K., Sadowy, G., Jones, C., Shaffer, S., Zebker, H., & Smith, R. (2008, May). The UAVSAR instrument: Description and first results. In 2008 IEEE Radar Conference (pp. 1-6). IEEE. DOI: 10.1109/RADAR.2008.4720722

Hetland, R.D., DiMarco, S.F., (2008). The effects of bottom oxygen demand in controlling the structure of hypoxia on the Texas–Louisiana continental shelf. J Mar Syst;70:49–62

Horstman, E.M., Dohmen-Janssen, C.M., Bouma, T.J., and Hulscher, S.J.M.H., (2015). Tidal-scale flow routing and sedimentation in mangrove forests: combining field data and numerical modelling. Geomorphology 228, 244–262. doi: 10.1016/j.geomorph.2014.08.011

Jensen, D., Simard, M., Cavanaugh, K., Sheng, Y., Fichot, C.G., Pavelsky, T., and Twilley, R., (2019). Improving the transferability of suspended solid estimation in wetland and deltaic waters with an empirical hyperspectral approach. 385 Remote Sensing, 11 . doi: 10.3390/RS11131629

Jensen, D.J., Cavanaugh, K.C., Thompson, D.R., Fagherazzi, S., Cortese, L., & Simard, M., (2022). Leveraging the historical Landsat catalog for a remote sensing model of wetland accretion in coastal Louisiana. Journal of Geophysical Research: Biogeosciences, 127, e2022JG006794. https://doi.org/10.1029/2022JG006794Received 12

Jensen, D.J., Castaneda-Moya, E. , Solohin, E., Rovai, A., Thompson, D.R., and Simard, M., (2023), Delta-X: AVIRIS-NG L3 Derived Aboveground Biomass, MRD, Louisiana, USA, 2021, V2. ORNL DAAC, Oak Ridge, Tennessee, USA. [Dataset]. https://doi.org/10.3334/ORNLDAAC/2138

Jensen, D., Thompson, D., Simard, M., Solohin, E., and Castañeda-Moya, E., (2023). Imaging spectroscopy-based estimation of aboveground biomass in Louisiana's coastal wetlands: Towards consistent spectroscopic retrievals across atmospheric states. In review at Remote Sensing of Environment.

Jones, C., Oliver-Cabrera, T., Varugu, B., Simard, M., and Lou., Y., (2022), Delta-X: UAVSAR L3 Water Level Changes, MRD, Louisiana, 2021. ORNL DAAC, Oak Ridge, Tennessee, USA. [Dataset]. https://doi.org/10.3334/ORNLDAAC/2058.

Leonardi, N., Carnacina, I., Donatelli, C., Ganju, N.K., Plater, A.J., Schuerch, M., and Temmerman, S., (2018), Dynamic interactions between coastal storms and salt marshes: A review: Geomorphology, v. 301, p. 92–107, https://doi.org/10.1016/ j.geomorph.2017.11.001.

Liao, T.H., Simard, M., Marshak, C., Denbina, M.W., (2019). Mapping mangrove extent and canopy height in gabon using interferometric coherence and Freeman-Durden decomposition from L-band ALOS/PALSAR-2. AGUFM 2019, H43N–2273.

Lu, Z., & Kwoun, O.I., (2008). Radarsat-1 and ERS InSAR analysis over southeastern coastal Louisiana: Implications for mapping water-level changes beneath swamp forests. IEEE Transactions on Geoscience and Remote Sensing, 46(8), 2167-2184.

Marani, M., D'Alpaos, A., Lanzoni, S., Carniello, L., & Rinaldo, A. (2007). Biologically-controlled multiple equilibria of tidal landforms and the fate of the Venice lagoon. Geophysical Research Letters,34, L11402. https://doi.org/10.1029/2007GL030178

Marani, M., D'Alpaos, A., Lanzoni, S., Carniello, L., & Rinaldo, A. (2010). The importance of being coupled: Stable states and catastrophic shiftsin tidal biomorphodynamics.Journal of Geophysical Research,115, F04004. https://doi.org/10.1029/2009JF001600

Marani, M., D'Alpaos, A., Lanzoni, S., & Santalucia, M., (2011), Understanding and predicting wave erosion of marsh edges. Geophysical Research Letters, 38, L21401. https://doi.org/10.1029/2011GL048995

Mariotti, G., and Fagherazzi, S., (2010), A numerical model for the coupled long-term evolution of salt marshes and tidal flats: Journal of Geophysical Research, v. 115, F01004, https://doi .org/10.1029/2009JF001326.

Mariotti, G., and Fagherazzi, S., (2013), Critical width of tidal flats triggers marsh collapse in the absence of sea-level rise: Proceedings of the National Academy of Sciences of the United States of America, v. 110, p. 5353–5356, https:// doi.org/10.1073/pnas.1219600110.

Mariotti, G., (2016). Revisiting salt marsh resilience to sea level rise: Are ponds responsible for permanent land loss? Journal of Geophysical Research: Earth Surface, 121, 1391– 1407. https://doi.org/10.1002/2016JF003900

Mazda, Y., Magi, M., Kogo, M., and Hong, P.N., (1997), Mangroves as a coastal protection from waves in the Tong King Delta, Vietnam. Mangroves and Salt Marshes 1:127–135

Medeiros, S., Hagen, S., Weishampel, J., Angelo, J., (2015). Adjusting lidar-derived digital terrain models in coastal marshes based on estimated aboveground biomass density. Remote Sens. (Basel) 7 (4), 3507–3525. https://doi.org/10.3390/rs70403507

Montgomery, J.M., Bryan, K.R., Horstman, E.M., Mullarney, J.C., (2018). Attenuation of tides and surges by mangroves: contrasting case studies from New Zealand. Water 10:1119

Morris, J.T., Barber, D.C., Callaway, J.C., Chambers, R., Hagen, S.C., Hopkinson, C.S., Johnson, B.J., Megonigal, P., Neubauer, S.C., Troxler, T. and Wigand, C., (2016). Contributions of organic and inorganic matter to sediment volume and accretion in tidal wetlands at steady state. Earth's future, 4(4), pp.110-121

Mudd, S. M., D'Alpaos, A., & Morris, J. T. (2010). How does vegetation affect sedimentation on tidal marshes? Investigating particle captureand hydrodynamic controls on biologically mediated sedimentation. Journal of Geophysical Research,115, F03029. https://doi.org/10.1029/2009J

Nepf, HM., (2012), Flow and transport in regions with aquatic vegetation. Annu. Rev. Fluid Mech. 44:123–42

Oliver-Cabrera, T., Wdowinski, S., (2016), InSAR-based mapping of tidal inundation extent and amplitude in Louisiana coastal wetlands. Remote Sens. (Basel) 8 (5), 393. https://doi.org/10.3390/rs8050393

Oliver-Cabrera, T., Jones, C.E., Yunjun, Z. Simard, M. (2021). InSAR Phase Unwrapping Error Correction for Rapid Repeat Measurements of Water Level Change in Wetlands. IEEE Trans. Geosci. Remote Sensing. DOI: 10.1109/TGRS.2021.3108751

Orton, P.M., Sanderson E.W., Talke, S.A., Giampieri, M., MacManus, K., (2020). Storm tide amplification and habitat changes due to urbanization of a lagoonal estuary. Nat. Hazards Earth Syst. Sci. 20:2415–32

Pannozzo, N., Leonardi, N., Carnacina, I., Smedley, R., (2021), Salt marsh resilience to sea-level rise and increased storm intensity. Geomorphology 389, 107825. https://doi. org/10.1016/j.geomorph.2021.107825

Pelckmans, I., Belliard, J.P., Dominguez-Granda, L.E., Slobbe, C., Temmerman, S., and Gourgue, O., (2023). Mangrove ecosystem properties regulate high water levels in a river delta, EGUsphere [preprint], https://doi.org/10.5194/egusphere-2023-428.

Peteet, D. M., Nichols, J., Kenna, T., Chang, C., Browne, J., Reza, M., et al., (2018), Sediment starvation destroys New York City marshes' resistance to sea level rise. Proceedings of the National Academy of Sciences, 115(41), 10,281–10,286. https://doi.org/10.1073/ pnas.1715392115

Reed, D.J., (1989). Patterns of sediment deposition in subsiding coastal salt marshes, Terrebonne Bay, Louisiana: The role of winter storms. Estuaries 12, 222-227

Rogers, J.N., Parrish, C.E., Ward, L.G., Burdick, D.M., (2018). Improving salt marsh digital elevation model accuracy with full-waveform lidar and nonparametric predictive modeling. Estuarine, Coast. Shelf Sci. 202, 193–211. https://doi.org/10.1016/j. ecss.2017.11.034

Rosen, P.A., Hensley, S., Joughin, I.R., Li, F.K., Madsen, S.N., Rodriguez, E., and Goldstein, R. M., (2000). Synthetic apertureradar interferometry,Proc. IEEE,88, 333–382

Rosen, P.A., Hensley, S., Wheeler, K., Sadowy, G., Miller, T., Shaffer, S., Madsen, S., (2006), UAVSAR: a new NASA airborne SAR system for science and technology research. In: 2006 IEEE Conference on Radar. IEEE. https://doi.org/10.1109/ RADAR.2006.1631770, 8-pp.

Schuerch, M., et al., (2018), Future response of global coastal wetlands to sea-level rise: Nature, v. 561, p. 231–234, https://doi.org/10.1038/s41586-018- 0476-5. Schwimmer, R.A., and Pizzuto, J.E., 2000, A model for the evolution of marsh shorelines: Journal of Sedimentary Research, v. 70, p. 1026–1035, https://doi.org/10.1306/030400701026

Sullivan, J.C., Torres, R., Garrett, A., (2019). Intertidal creeks and overmarsh circulation in a small salt marsh basin. J. Geophys. Res. Earth Surf. 124:447–63

Tas, S.A.J., van Maren, D.S., and Reniers, A.J.H.M. (2022). Chenier formation through wave winnowing and tides. Journal of Geophysical Research: Earth Surface, 127, e2022JF006792, https://doi.org/10.1029/2022JF006792

Temmerman, S., Bouma, T.J., Govers, G., and Lauwaet, D., (2005), Flow paths of water and sediment in a tidal marsh: Relations withmarsh developmental stage and tidal inundation height, Estuaries,28(3), 338–352, doi:10.1007/BF02693917

Temmerman, S., Meire, P., Bouma, T.J., Herman, P.M.J., Ysebaert, T., and De Vriend, H.J., (2013), Ecosystem-based coastal defence in the face of global change: Nature, v. 504, p. 79–83, https:// doi.org/10.1038/nature12859.

Temmerman, S., Horstman, E.M., Krauss, K.W., Mullarney, J.C., Pelckmans, I., Schoutens, K., (2022). Marshes and Mangroves as Nature-Based Coastal Storm Buffers. Annu. Rev. Mar. Sci., 15, 95–118

Thompson, D.R., Cawse-Nicholson, K., Erickson, Z., Fichot, C.G., Frankenberg, C., Gao, B.-C., Gierach, M.M., Green, R.O., Jensen, D., Natraj, V., and Thompson, A., (2019). A unified approach to estimate land and water reflectances with uncertainties for coastal imaging spectroscopy. Remote Sensing of Environment 231:111198. https://doi.org/10.1016/j.rse.2019.05.017

Thompson, D.R., D.J. Jensen, J.W. Chapman, M. Simard, and E. Greenberg. 2022. Delta-X: AVIRIS-NG BRDF-Adjusted Surface Reflectance, MRD, LA, 2021. ORNL DAAC, Oak Ridge, Tennessee, USA. https://doi.org/10.3334/ORNLDAAC/2025

Wiberg, P.L., Fagherazzi, S., Kirwan, M.L., (2020). Improving predictions of salt marsh evolution through better integration of data and models. Ann. Rev. Mar. Sci. 12, 389–413. https://doi.org/10.1146/annurev-marine-010419-010610

Winterwerp, J.C., Albers, T., Anthony, E.J., Friess, D.A., Mancheño, A.G., Moseley, K., (2020). Managing erosion of mangrove-mud coasts with permeable dams–lessons learned. Ecol Eng.; 158

Wright, K., Passalacqua, P., Simard, M., & Jones, C.E., (2022). Integrating connectivity into hydrodynamic models: An automated open-source method to refine an unstructured mesh using remote sensing. Journal of Advances in Modeling Earth Systems, 14(8), e2022MS003025

Wu, Y., Thorne, E.T., Sharp, R.E., Cosgrove, D.J., (2001) Modification of expansin transcript levels in the maize primary root at low water potentials. Plant Physiol., 126, 1471–1479

Xie, D., Schwarz, C., Kleinhans, M.G., Zhou, Z., van Maanen, B., (2022). Implications of coastal conditions and sea-level rise on mangrove vulnerability: A bio-morphodynamic modeling study. J. Geophys. Res.: Earth Surf. 127(3), e2021JF006301. https://doi.org/10.1029/2021JF006301

Xu, Y., Kalra, T. S., Ganju, N. K., and Fagherazzi, S. (2022). Modeling the dynamics of salt marsh development in coastal land reclamation. Geophysical Research Letters, 49(6), e2021GL095559. https://doi.org/10.1029/2021GL095559

Zhang, X., Jones, C.E., Oliver-Cabrera, T., Simard, M., and Fagherazzi, S., (2022a). Using rapid repeat SAR interferometry to improve hydrodynamic models of food propagation in coastal wetlands, Advances in Water Resources, vol. 159, Article ID 104088

Zhang, X., Wright, K., Passalacqua, P., Simard, M., and Fagherazzi, S., (2022b). Improving channel hydrological connectivity in coastal hydrodynamic models with remotely sensed channel networks, Journal of Geophysical Research: Earth Surface, vol. 127

Figure 1.

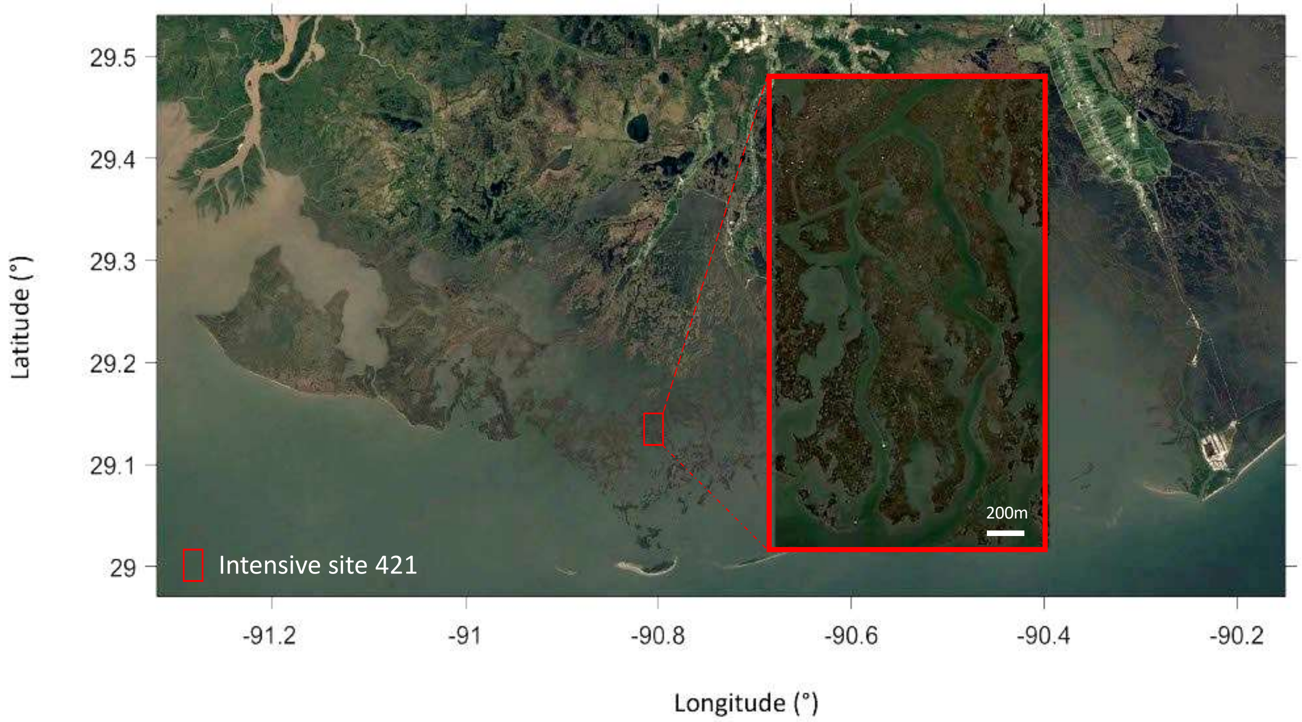
29.5
29.4
29.3
29.2
29.1
29
Latitude (°)
200m
Intensive site 421
-91.2
-91
-90.8
-90.6
-90.4
-90.2
Longitude (°)

Figure 1

Figure 2.

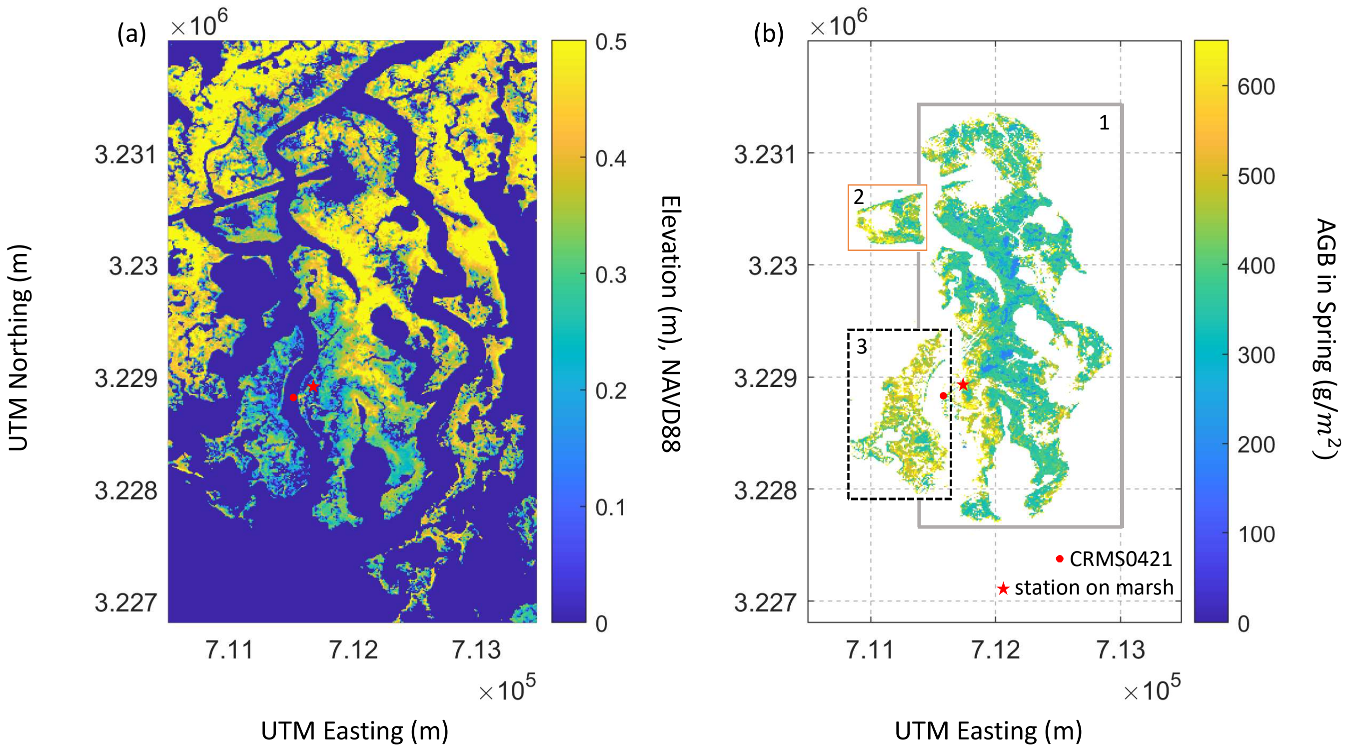
(a)
×10^6
3.231
3.23
3.229
3.228
3.227
UTM Northing (m)
7.11
7.12
7.13
×10^5
UTM Easting (m)
0.5
0.4
0.3
0.2
0.1
0
Elevation (m), NAVD88
(b)
×10^6
1
2
3
3.231
3.23
3.229
3.228
3.227
CRMS0421
station on marsh
7.11
7.12
7.13
×10^5
UTM Easting (m)
600
500
400
300
200
100
0
AGB in Spring (g/m^2)

Figure 2

Figure 3.

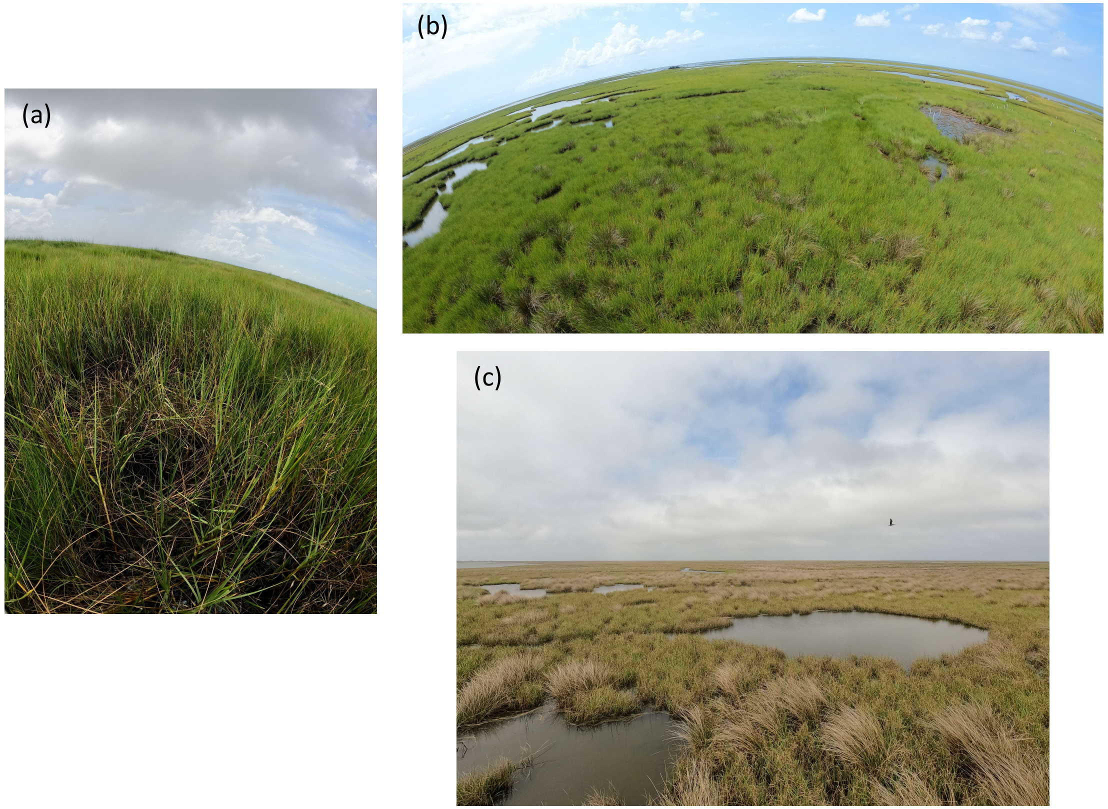

Figure 3

Figure 4.

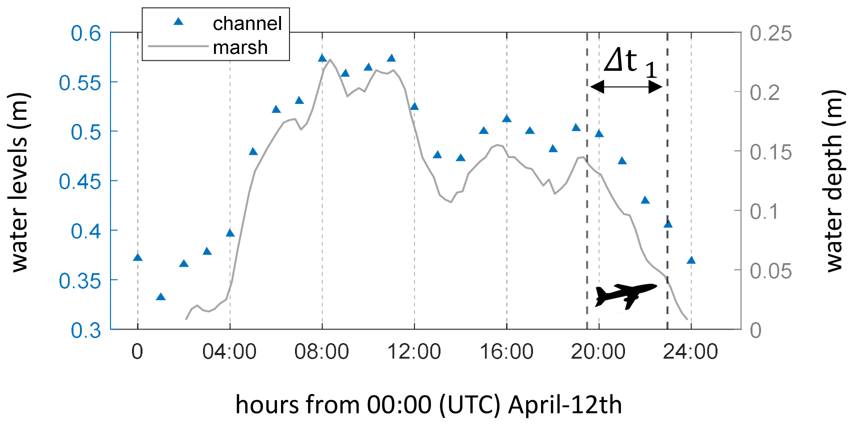
channel
marsh
Δt 1
water levels (m)
water depth (m)
0.6
0.55
0.5
0.45
0.4
0.35
0.3
0.25
0.2
0.15
0.1
0.05
0
0
04:00
08:00
12:00
16:00
20:00
24:00
hours from 00:00 (UTC) April-12th

Figure 4

Figure 5.

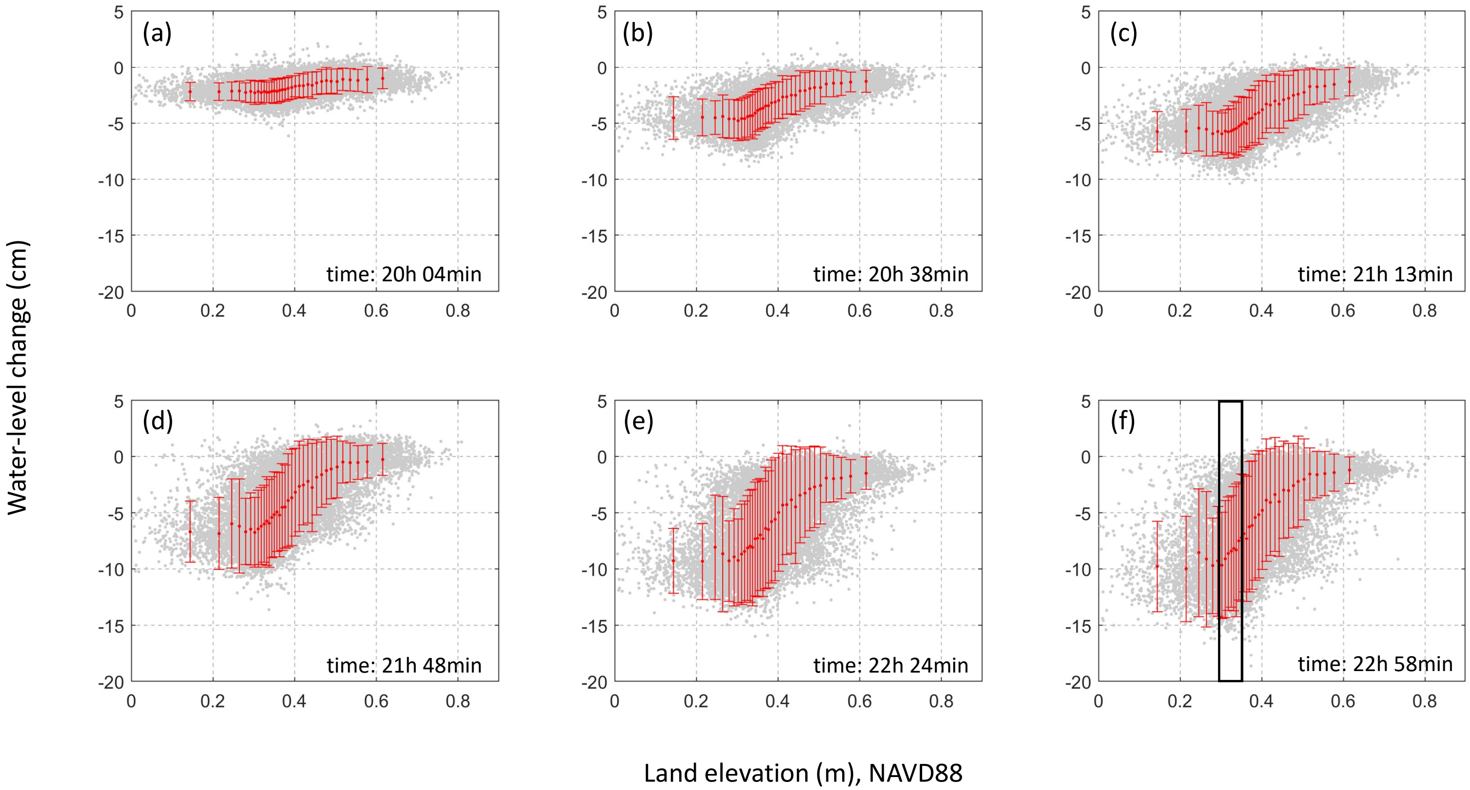

(a)
time: 20h 04min
(b)
time: 20h 38min
(c)
time: 21h 13min
(d)
time: 21h 48min
(e)
time: 22h 24min
(f)
time: 22h 58min
Water-level change (cm)
Land elevation (m), NAVD88

Figure 5

Figure 6.

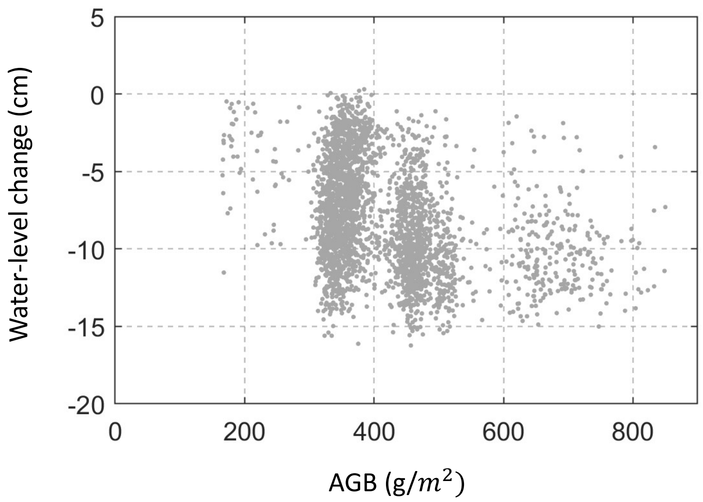

Figure 6

Figure 7.

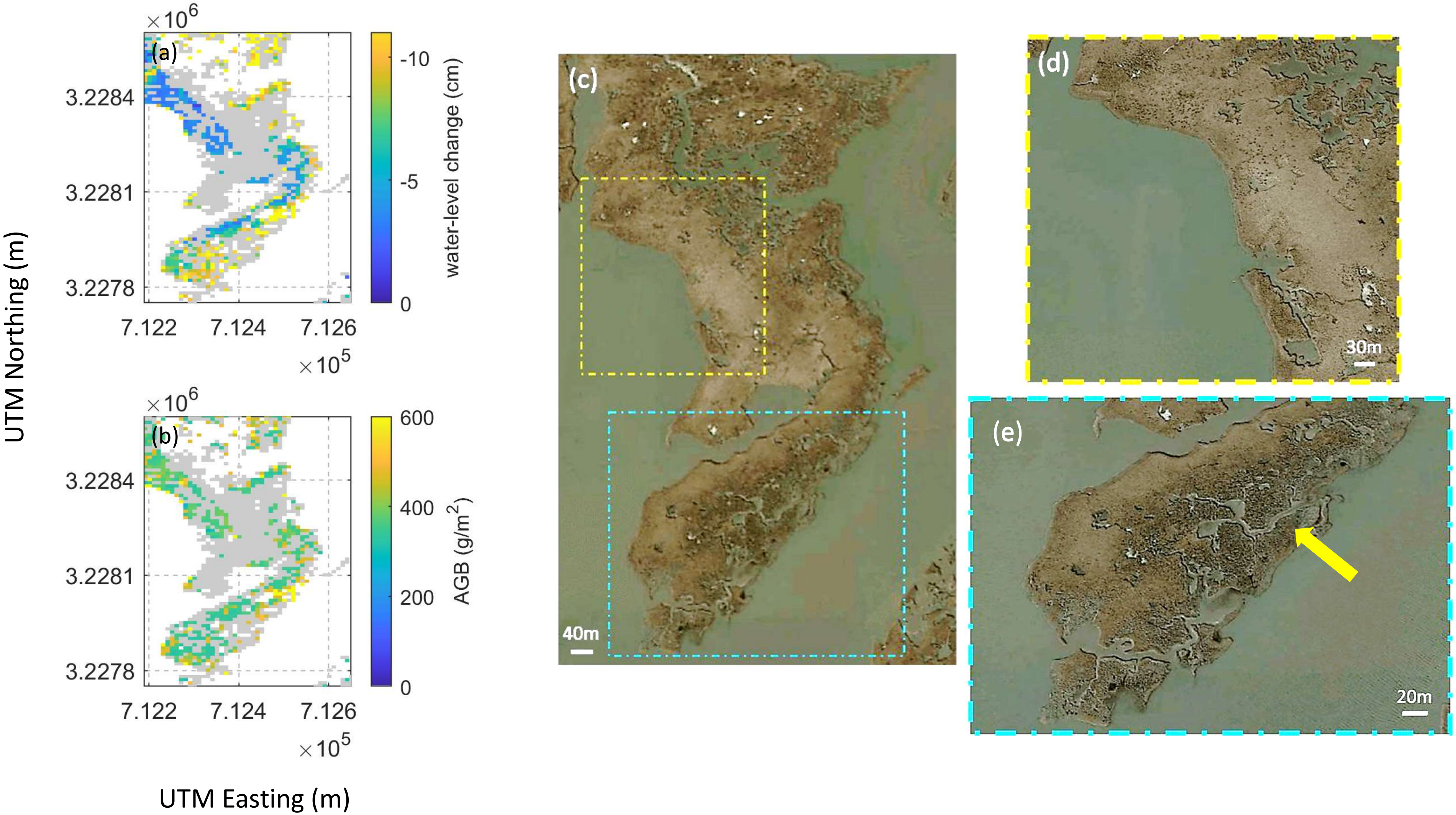

(a)
(b)
(c)
(d)
(e)
UTM Northing (m)
UTM Easting (m)
water-level change (cm)
AGB (g/m^2)
40m
30m
20m

Figure 7

Figure 8.

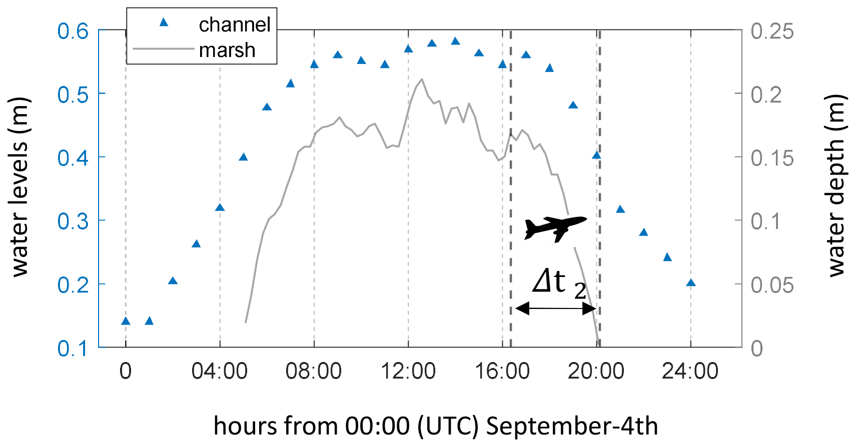

channel
marsh
0.6
0.5
0.4
0.3
0.2
0.1
water levels (m)
0.25
0.2
0.15
0.1
0.05
0
water depth (m)
Δt 2
0
04:00
08:00
12:00
16:00
20:00
24:00
hours from 00:00 (UTC) September-4th

Figure 8

Figure 9.

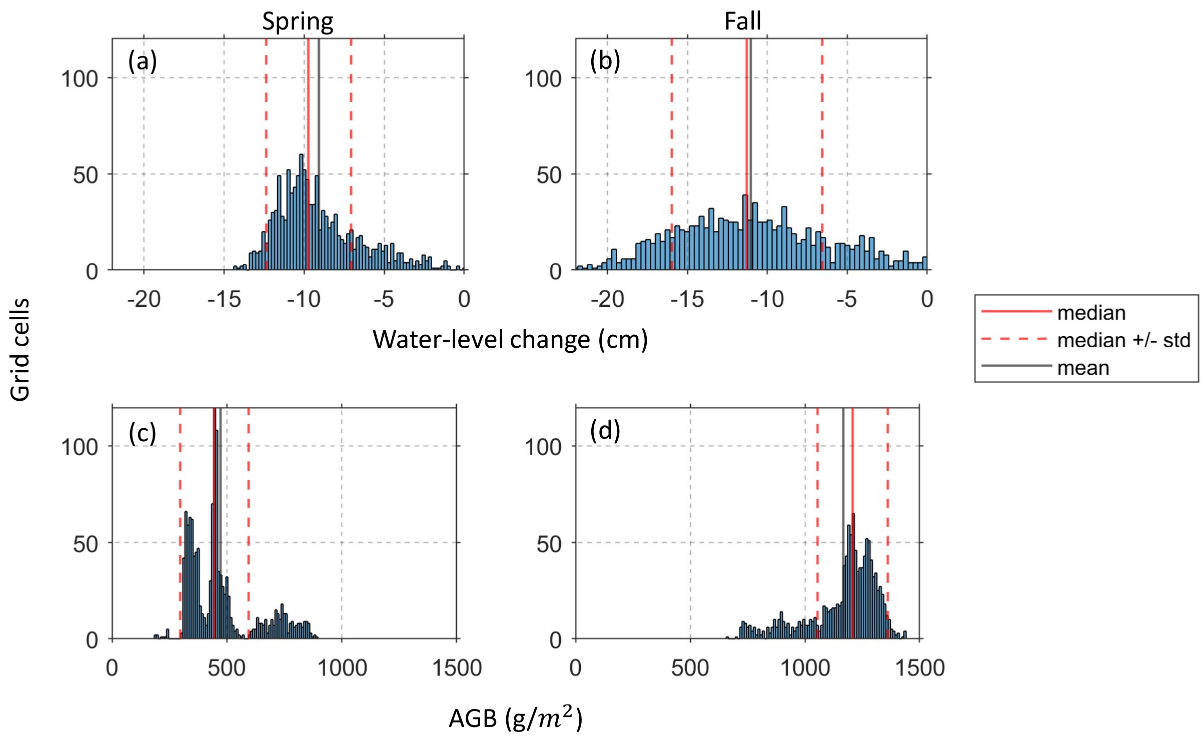
Spring
Fall
(a)
(b)
(c)
(d)
100
50
0
-20
-15
-10
-5
0
Grid cells
Water-level change (cm)
median
median +/- std
mean
500
1000
1500
AGB (g/m^2)

Figure 9

Figure 10.

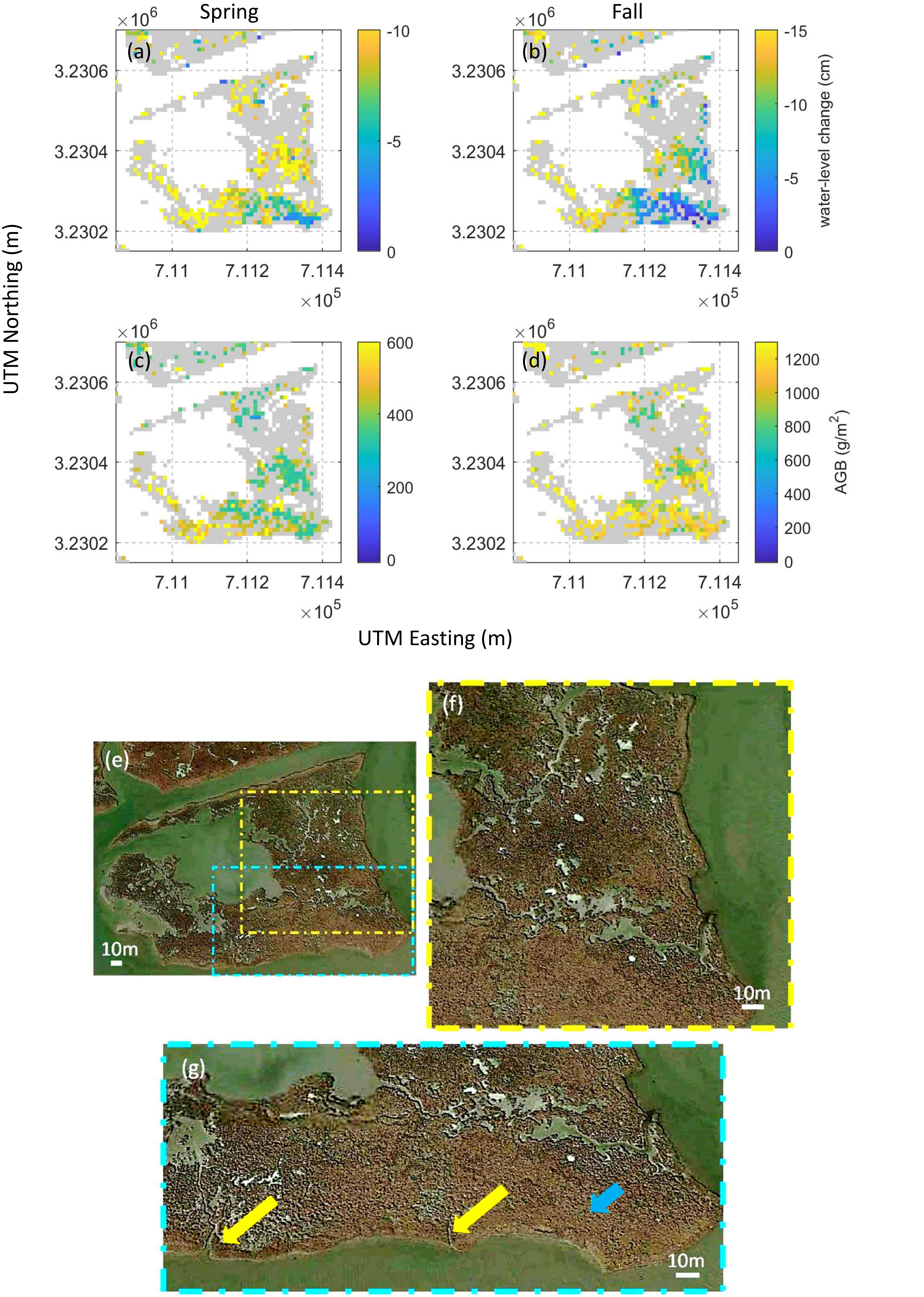

Spring
Fall
(a)
(b)
(c)
(d)
(e)
(f)
(g)
UTM Northing (m)
UTM Easting (m)
water-level change (cm)
AGB (g/m^2)
10m

Figure 10

Figure 11.

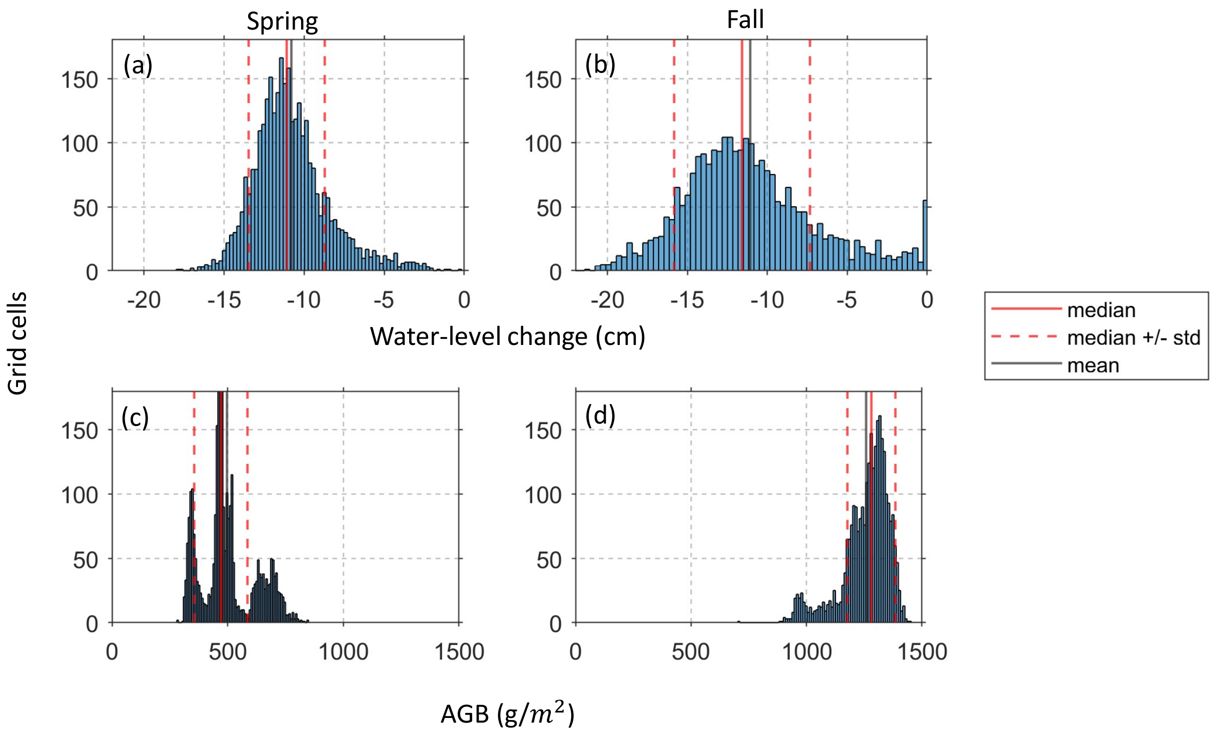
Spring
Fall
(a)
(b)
(c)
(d)
Grid cells
Water-level change (cm)
AGB (g/m^2)
median
median +/- std
mean

Figure 11

Figure 12.

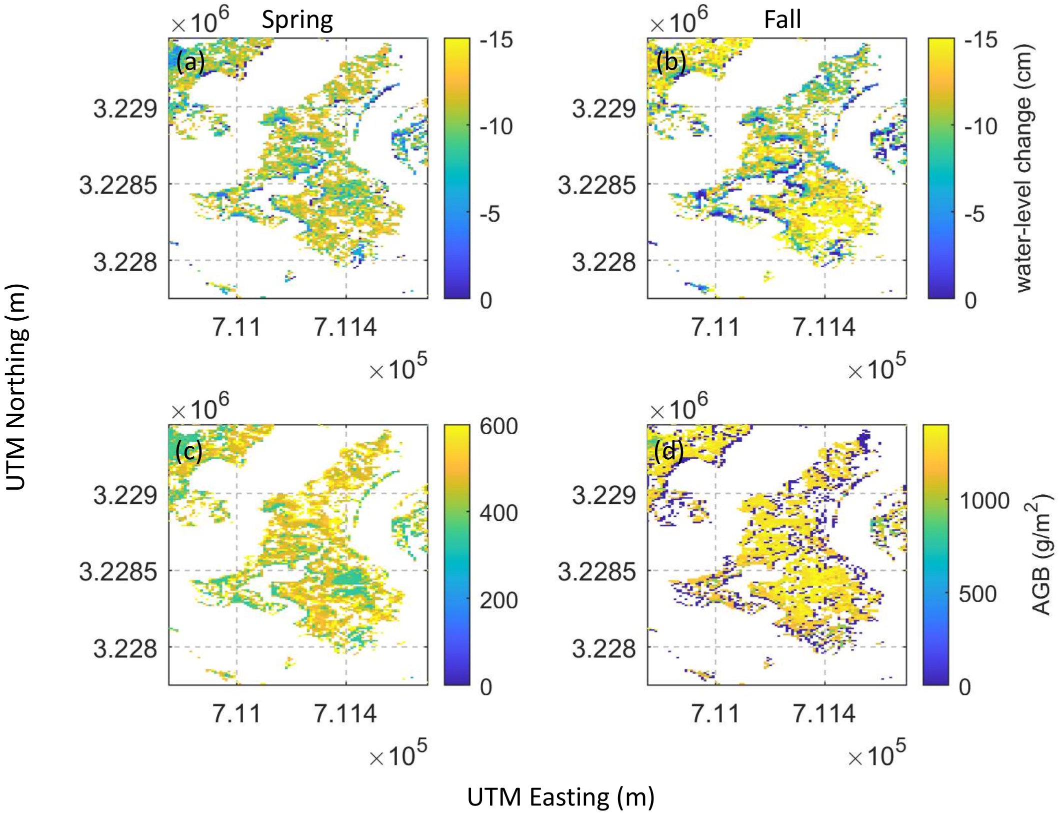

Spring
Fall
(a)
(b)
(c)
(d)
3.229
3.2285
3.228
7.11
7.114
$\times 10^6$
$\times 10^5$
-15
-10
-5
0
water-level change (cm)
600
400
200
1000
500
AGB (g/m^2)
UTM Northing (m)
UTM Easting (m)

Figure 12

Figure 13.

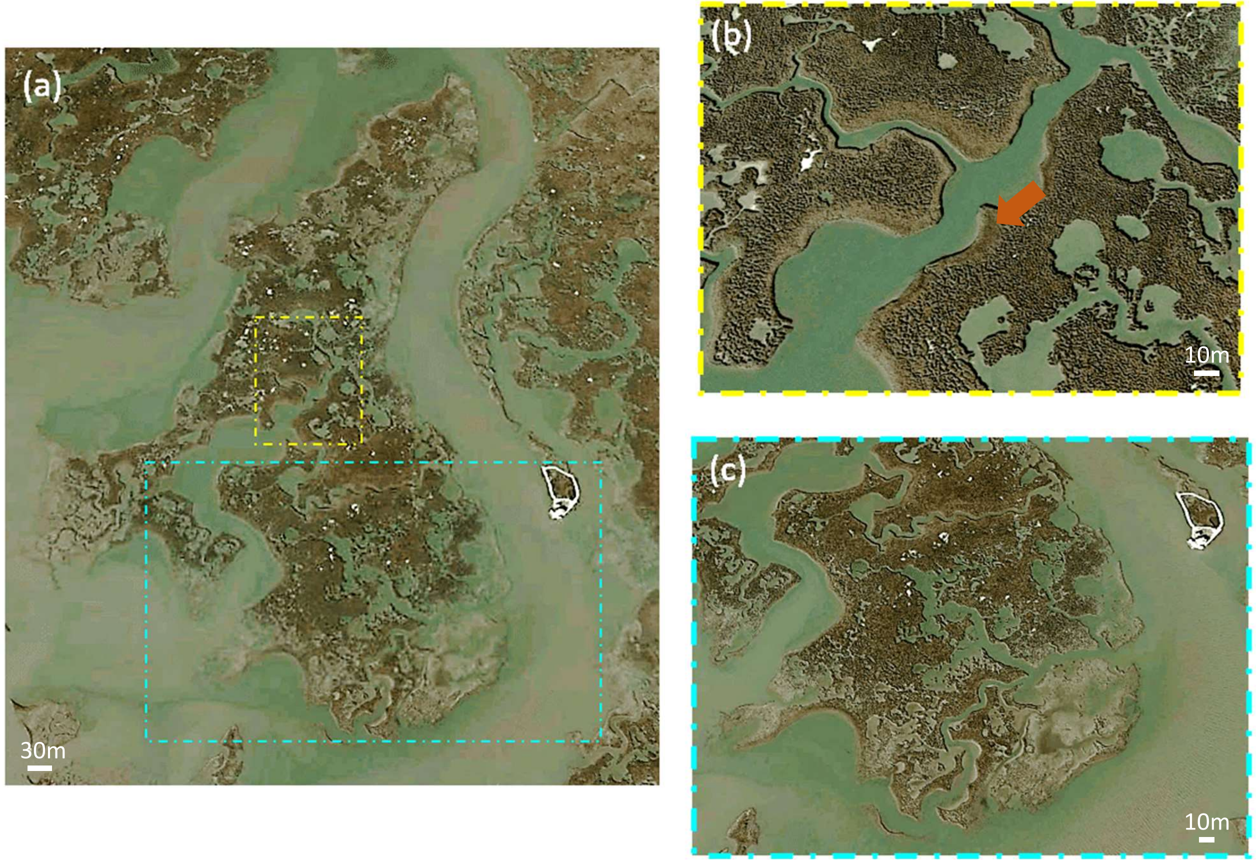

Figure 13

		Height (cm)	Diameter (cm)	Density (stems/m^2)
Supratidal S. alterniflora (spring)	AGB	48.71	4.52	112
Supratidal S. alterniflora (spring)	AGN	46.62	6.03	128
Supratidal S. alterniflora (fall)	AGB	72.4	6.5	304
Supratidal S. alterniflora (fall)	AGN	44.3	6.17	48

Table 1. Mean height, mean stem diameter, and stem density (latitude 29.1714, longitude 90.8223). The data were collected between 2021-03-21 to 2021-03-31 during the Delta-X Spring 2021 deployment, and between 2021-08-19 to 2021-08-27 during the Fall deployment.

	Median	Mean	Standard deviation	Interquartile range	Skewness
Water-level change (cm), campaign 1	-9.73	-9.08	2.68	3.32	0.91
AGB (g/cm^2), spring	445	473	148	145	1.10
Water-level change (cm), campaign 2	-11.28	-11.05	4.69	6.61	0.18
AGB (g/cm^2), fall	1208	1168	154	159	-1.20

Table 2. Mean, median, standard deviation, interquartile range, and skewness of WLC (cm) and AGB (g/cm^2) on marsh 2 (see Figure 2b).

	Median	Mean	Standard deviation	Interquartile range	Skewness
Water-level change (cm), campaign 1	-11.10	-10.79	2.38	2.66	0.88
AGB (g/cm^2), spring	471	497	114	83	0.61
Water-level change (cm), campaign 2	-11.58	-11.08	4.25	5.14	0.56
AGB (g/cm^2), fall	1281	1257	103	117	-1.28

Table 3. Mean, median, standard deviation, interquartile range and skewness of WLC (cm) and AGB (g/cm^2) on marsh 3 (see Figure 2b).